Engineering Failure Analysis 175 (2025) 109566

Contents lists available at ScienceDirect

Engineering Failure Analysis

journal homepage: www.elsevier.com/locate/engfailanal

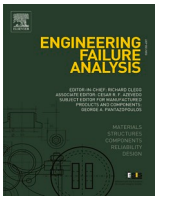

Corrosion protective performance evaluation of structural aircraft coatings in cyclic salt spray, outdoor and In-Service environments

A.J. Cornet [a,b,*], A.M. Homborg [a,c], L.'t Hoen-Velterop [d], J.M.C Mol [a]

[a] Department of Materials Science and Engineering, Delft University of Technology, Mekelweg 2, 2628 CD Delft, the Netherlands
[b] Royal Netherlands Air Force, Kooiweg 40, 4631SZ Hoogerheide, the Netherlands
[c] Netherlands Defence Academy, Het Nieuwe Diep 8, 1781AC Den Helder, the Netherlands
[d] Royal Netherlands Aerospace Centre NLR, Voorsterweg 31, 8316PR Marknesse, the Netherlands

ARTICLE INFO

Keywords:
Aluminium Alloy
Organic coatings
Outdoor exposure
Cyclic salt spray test
In-service aging
Corrosion

ABSTRACT

Eliminating hexavalent chromium-based corrosion inhibitors from structural aircraft coatings remains a significant challenge, primarily due to the lack of reliable accelerated test methods. This study evaluates the performance of various structural aircraft coatings under different exposure conditions, i.e. outdoor exposure, cyclic salt spray testing and in-service conditions, supplemented by environmental sensors. Quarterly inspections and scanning electron microscopy were used to evaluate corrosion damage. The findings highlight a lack of correlation between accelerated testing and outdoor exposure testing, likely driven by disparities in salt deposition, UV-radiation, time of wetness and temperature cycling. Additionally, galvanic couples between skin and fasteners remain difficult to protect, with chromate-based systems offering limited inhibition and alternative systems struggling to protect such complex assemblies. However, in lap-joints, alternative coatings outperformed chromate-based counterparts, likely due to their polymer matrices providing improved barrier properties, hence limiting access of electrolyte to the coating-aluminium alloy interface.

1. Introduction

Since the early days of aviation in the 1920 s, the aerospace industry has experienced a remarkable evolution. The initial drive behind aircraft development was a quest for flight itself, with pioneers experimenting, innovating, and gradually combining complex technologies to achieve sustained flight. However, early designs were highly unreliable, resulting in frequent accidents and underscoring the urgent need for safer, more reliable aircraft. By the 1940 s, aviation priorities began to shift toward reliability and ensuring flight safety. This shift spurred the development of standards and regulations within the aerospace industry aiming at a guaranteed quality and performance of materials [1].

Part of this regulatory framework involved creating standards for organic coatings to protect aircraft structures from corrosion. These aviation standards for organic coatings set stringent performance criteria, focusing on properties such as corrosion resistance, adhesion, fluid resistance, strippability and flexibility [2,3]. From the beginning, these standards concentrated on chromate-containing coating systems, as chromates had become the backbone of corrosion protection for aircraft structures [4]. Over decades, both

* Corresponding author at: Department of Materials Science and Engineering, Delft University of Technology, Mekelweg 2, 2628 CD Delft, The Netherlands.
E-mail address: A.J.Cornet@TUDelft.nl (A.J. Cornet).

https://doi.org/10.1016/j.engfailanal.2025.109566
Received 6 February 2025; Received in revised form 7 March 2025; Accepted 25 March 2025
Available online 29 March 2025

empirical studies and historical performance data confirmed that chromate-based coatings provided sufficient protection, maintaining the structural integrity of aircraft throughout their service lives and thereby contributing to airworthiness.

Despite their efficacy, chromate compounds pose serious environmental and health risks, being both toxic and carcinogenic [5,6]. This has driven decades of research focused on eliminating chromate-based inhibitors from coating systems [7–10]. Through this extensive research, significant insightful progress has been made: (i) potential alternative corrosion inhibitors have been identified [11–13]; (ii) a more comprehensive understanding of corrosion degradation of aerospace aluminium alloys, including the protection mechanisms of chromate-based coatings and their proposed alternatives, has been gained [14–16] and (iii) discrepancies in test results between accelerated ageing tests and performance during service have been identified [16–19].

Efforts to improve accelerated corrosion testing have led to the advancement of the neutral salt spray test into various cyclic salt spray test (CSST) protocols [14,16,20,21]. These protocols incorporate repeated cycles of humidity, temperature fluctuations, UV radiation and exposure to chloride-rich aerosols (based on artificial sea-salt solutions) to better simulate real in-service environments. As a result, CSSTs have demonstrated improved correlation with natural weathering, making these particularly valuable for evaluating exterior aircraft coating systems (which typically consist of a top coat, primer and pre-treatment) [22]. This is reflected in SAE AMS 3095, which relies on CSST results for coating qualification. By contrast, MIL-PRF-32239 mandates a one-year outdoor exposure test to benchmark new coating systems against chromate-based references. This reflects concerns over CSST's ability to predict long-term performance in military contexts where exterior coatings must endure extended service, often without frequent external coating replacements whereas in civil aviation, regular repainting of aircraft exteriors is standard practice [16,19,23].

While accelerated testing is valuable for evaluating external aircraft coatings, it does not fully replicate the complex and prolonged exposure conditions encountered for structural aircraft coatings (which typically consist of one layer of primer over a pre-treatment) [16,19,22]. These components are often in contact with aircraft fluids, receive little to no UV radiation and incorporate dissimilar materials, e.g. at joints and fasteners. As a result, these interfaces are often exposed to mechanical stresses and electrochemical interactions [24]. These factors make structural components particularly susceptible to galvanic corrosion, filiform corrosion, crevice corrosion and blistering of protective coatings [24]. Since current accelerated test methods do not fully capture these unique environmental stressors, CSST results alone are insufficient for predicting long-term performance of chromate-free coatings for structural applications [16,19]. This is further complicated by a limited understanding of specific degradation mechanisms in these environments. Consequently, achieving long-lasting corrosion protection for structural aircraft parts, without relying on chromate-based inhibitors, remains a significant challenge for the aerospace industry.

In response to these challenges, this study investigates the performance of various structural coating systems across a range of test environments, focusing on the corrosion failure mechanisms induced by environmental factors. To identify the root causes of these failure mechanisms, environmental data were collected using sensors and weather stations, including data from the Royal Netherlands Meteorological Institute (KNMI), and were compared to corrosion and degradation observed through periodic visual inspections and scanning electron microscopy (SEM) analysis. The study also proposes measures to (i) improve the correlation between artificial aging tests and real-world conditions and (ii) mitigate corrosion at lap-joints in modern aircraft structures through the application of specific barrier coatings. In doing so, the authors offer deeper insights into current corrosion challenges, particularly around fasteners and at the interfaces between Carbon Fibre Reinforced Polymer (CFRP) materials and aluminium alloys, which are used in modern aircraft structures such as the A350, B787, and F-35. Future work will further quantify the degradation of coatings by using electrochemical and spectroscopic techniques, though this is beyond the scope of the present study.

2. Methodology

2.1. Test samples

This study compares four different coating systems: two chromate-containing systems used as reference and two commercially available alternatives, specifically a praseodymium-based coating and a lithium-based coating. These systems—comprising a primer-only configuration combined with pre-treatment—are designed for structural applications, where replacing chromates is particularly challenging because of the long service life requirements for the aircraft interior.

The coatings were applied with a dry coating thickness of approx. 25 μm on anodized AA2024-T62 substrates. AA2024-T62 is a heat-treated high-strength aluminium-copper alloy widely used in aerospace applications. Its composition includes approx. 4.5 % copper, 1.5 % magnesium, 0.6 % manganese with the remainder being aluminium (all in weight percent). Chromate-based systems were pre-treated using chromic acid anodizing, while the alternative systems were subjected to thin film sulfuric acid anodizing, both in accordance with MIL-A-8625. Table 1 provides detailed specifications of the coating systems and their respective pre-treatments.

The tests incorporated two chromate-based coating systems to facilitate the comparison of various accredited coating systems. The

Table 1
Coating systems under evaluation.

Coating system	Substrate material	Pre-treatment	Primer
Chromate-1	AA2024-T62	Chromic acid anodizing	$SrCrO_4$ epoxy polyamide primer
Chromate-2	AA2024-T62	Chromic acid anodizing	$SrCrO_4$ epoxy polyamide primer
Praseodymium	AA2024-T62	Thin Film Sulfuric Acid Anodizing	Praseodymium epoxy polyamide primer
Lithium	AA2024-T62	Thin Film Sulfuric Acid Anodizing	Lithium-phosphate polyurethane primer

chromate-1 system has been extensively studied in previous research, proving its effectiveness for structural applications after more than 35 years in service [25,26]. In contrast, the long-term performance of the chromate-2 system remains unexplored, even though it is accredited for the same application. This makes the chromate systems a valuable benchmark for evaluating long-term performance under the (accelerated) exposure conditions considered in this study. Furthermore, this approach could potentially be extended to estimate the long-term performance of alternative coating systems, such as the lithium- and praseodymium-based coatings under evaluation.

The coated panels were subjected to one of the three following exposure conditions:

i. Outdoor exposure for a duration of 2 years.
ii. Cyclic salt spray testing (CSST) for a duration of 1000 h.
iii. In-service exposure, for a duration of 2.5 years.

Efforts were made to maintain consistent panel configurations across all exposure conditions. However, aircraft panels used in flight tests were adjusted, making their configuration slightly different from those used in outdoor exposure and CSST. The various panel configurations are illustrated in Fig. 1.

All exposure panels included three types of rivets installed in X-scribed holes: titanium rivets (Ti-6Al-4V), stainless-steel rivets (A286) and bare aluminium rivets (AA2117-T4, with the chromate conversion coating removed using nitric acid). These rivets were installed dry, without paint or sealant, to maximize the galvanic corrosion effects. The panels were painted before assembly.

The rivets were used to assemble the components: to connect stiffeners to panels in the flight test samples and to combine three panels together for the outdoor and CSST exposure panels. These three panels comprised panel 1 and 2 (both 6″ x 4″ x 0.032″) combined with panel 3 (6″ x 2″ x 0.064″), together creating a lap-joint. Lap-joints are particularly prone to corrosion as water can become trapped between the adjacent surfaces. The combination of lap-joints with various types of rivets makes this configuration especially susceptible to corrosion due to the crevices between the panels and the galvanic effects arising from the different materials used in the joint.

Additionally, an X-scribe was applied on the coated substrates to evaluate the behaviour of different inhibitors inside a scratch without galvanic effects of fasteners. X-scribes were made with a lathe tool in accordance with ASTM-D1654.

For both outdoor exposure and CSST, two sets of panel assemblies were prepared. The first set, referred to as Al-Al coupled panels, consisted of three coated AA2024-T62 aluminium panels (panel 1, 2 and 3). The second set, referred to as Al-CFRP coupled panels, included a bare CFRP sheet, on one side insulated by a single glass fibre layer (panel 2) and sandwiched between two coated AA2024-T62 aluminium sheets (panel 1 and 3). This configuration is designed to investigate galvanic corrosion at CFRP-aluminium interfaces under the protection of chromium, praseodymium or lithium coating systems. This study is particularly relevant, as these interfaces are highly susceptible to corrosion in modern aerospace structures [27].

2.2. Test conditions

2.2.1. Outdoor exposure

The outdoor exposure lasted from 18 March 2022 to 18 March 2024, at Naval Air Station De Kooy in Den Helder, the Netherlands. Panels were mounted on an exposure rack attached to the air traffic control tower at a total elevation of 14 m, vertically oriented (90° with respect to the horizon) and facing south-southwest. Weather conditions were recorded by the KNMI and retrieved from their online database.

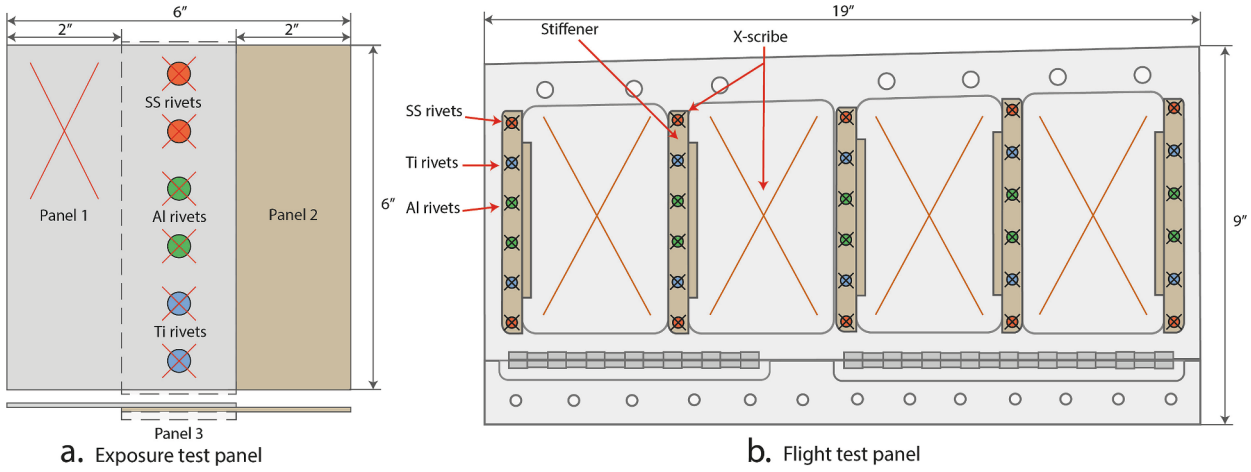

Fig. 1. Panel configuration; a) Panels used for outdoor exposure and cyclic salt spray testing, b) Example of a flight test panel (dimensions in inches).

For this study, 'winter' was defined as ranging from 15 October to 15 April and 'summer' from 15 April to 15 October. Day and night were determined based on sunrise and sunset times for De Kooy (coordinates: LON North 52.928, LAT East 4.781).

Since this study used only primer configurations, despite their intended application for structural use, UV radiation was expected to accelerate coating degradation to a certain extent. Consequently, the results from the outdoor exposure test, which includes natural UV radiation, may not directly align with those from CSST's or flight tests, where UV exposure is absent, which limits the applicability of the outdoor exposure test. Nevertheless, since the primary focuses of this study is on corrosion inhibition by active inhibitors within the coating systems rather than the overall coating degradation, the findings remain valuable. Therefore, the outdoor exposure test was incorporated into the experimental setup.

2.2.2. Cyclic salt spray test (CSST)

For the CSST, panels were placed at a 7° angle with respect to the vertical inside the salt spray cabinet. The panels were exposed to 500 cycles with the following test conditions:

I. High humidity period (1 h):
a. 15 min salt spray using an ASTM-D1193 Type IV artificial seawater solution acidified to pH 3 with HCl;
b. 45 min high humidity exposure (>80 % RH).
II. Dry-off period (1 h):
a. RH reduced to below 40 % for at least 35 min;
b. Ramp rate: RH reduced from 80 % to 40 % within 25 min.

The following cabinet settings were maintained during the test:

- Atomized nozzle pressure: 10–25 PSI
- Bubble tower temperature: 47 ℃
- Salt spray chamber temperature: 40 +/- 3 °C
- Fog collection rate: 1.0–2.0 ml/h continuous spray per 80 cm^2 (measured over at least 16 h using minimum 2 collectors)

The exposure conditions were logged using Luna Sensors (type: Acuity LS). The test protocol is based on the method developed by Dante et al [28].

2.2.3. Flight test

Three aircraft were outfitted with five test panels each: two praseodymium-based coatings, two lithium-based coatings and one containing the chromate-2 system. Over a 2.5 year period, the aircraft accumulated an average of 275 flight hours, with 1.5 flight hours equating to 1 cycle. Each cycle comprised one take-off, cruise and landing.

Unlike commercial aircraft which are designed for 60.000–100.000 flight hours, military aircraft typically fly only 6000 h over their lifespan and spend the majority of their time in shelters. To assess the impact of aircraft parking, Luna Sensors (Acuity LS) were installed in these shelters from 18 February 2022 to 9 January 2024 to monitor environmental conditions. This data was compared with KNMI data to evaluate shelter-induced corrosion effects.

Weather conditions at the Air Base were recorded by the KNMI from 18 February 2022 to 9 January 2024. The data were downloaded from the KNMI database. Winter was defined again as ranging from 15 October to 15 April and summer from 15 April to 15 October. Day and night were based on sunrise and sunset times for the Air Base.

2.3. Evaluation method

Outdoor exposure and flight test panels were visually inspected every three months during exposure. Detailed photographs were taken to document degradation and corrosion, particularly around scribed rivets and x-scribes without fasteners. During CSST, overview photos were taken on a weekly basis.

After exposure, stainless-steel rivets and x-scribe samples were analyzed using a Thermo Scientific™ Helios™ UXe DualBeam G4 SEM equipped with an Energy-Dispersive X-ray Spectroscopy (EDX) detector and a plasma Focused Ion Beam (FIB). The FIB was used to create cross-sections in the coating. This preparation step ensured that the inhibitors did not leach out due to contact with water during conventional sample preparation steps.

To prevent charging effects during SEM analysis, a carbon layer of approximately 20 nm thick was sputtered onto the sample surface prior to imaging.

3. Results and discussion

3.1. Exposure environments

Under various exposure conditions, environmental parameters such as temperature, relative humidity (RH), time of wetness (TOW), humidity cycles and salt deposition play critical roles in influencing material corrosion rates [29–32]. These parameters are difficult to control during outdoor exposure or operational use. However, during the CSST, both temperature and RH are regulated,

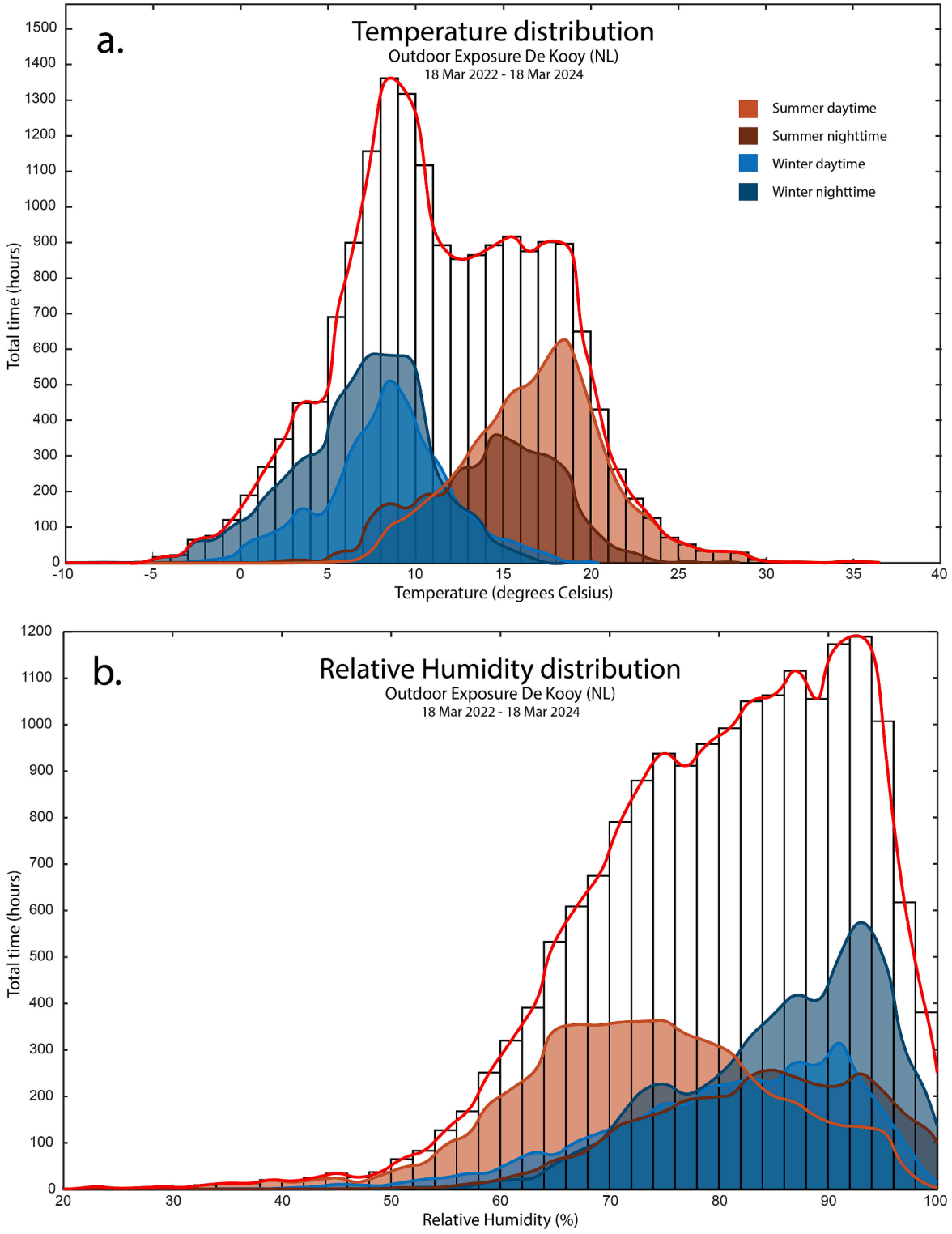

Fig. 2. Environmental data during the 2-year outdoor exposure test at Naval Air Station De Kooy: (a) temperature and (b) relative humidity variation over the exposure period, categorized by season and day- vs. nighttime conditions.

indirectly affecting the TOW. Additionally, salt deposition is standardized in the CSST by spraying an artificial seawater solution for a duration of 15 min in each cycle.

To better understand the environmental severity under these different conditions, data logging was employed to monitor corrosion-critical parameters during outdoor exposure, CSST and partly during operational service.

3.1.1. Outdoor exposure

During the outdoor exposure test, environmental parameters were logged by the KNMI. These data provided insights into temperature, RH and TOW. Fig. 2 presents this data as histograms of temperature and RH.

The first observation from Fig. 2 is the seasonal variation in temperature between summer and winter. In winter, the average temperature is 7.5 ± 12 °C, while in summer, it is 16 ± 13 °C. The average daytime temperature varies by approx. 2 to 3 °C compared to the average nighttime temperature, both in summer and winter.

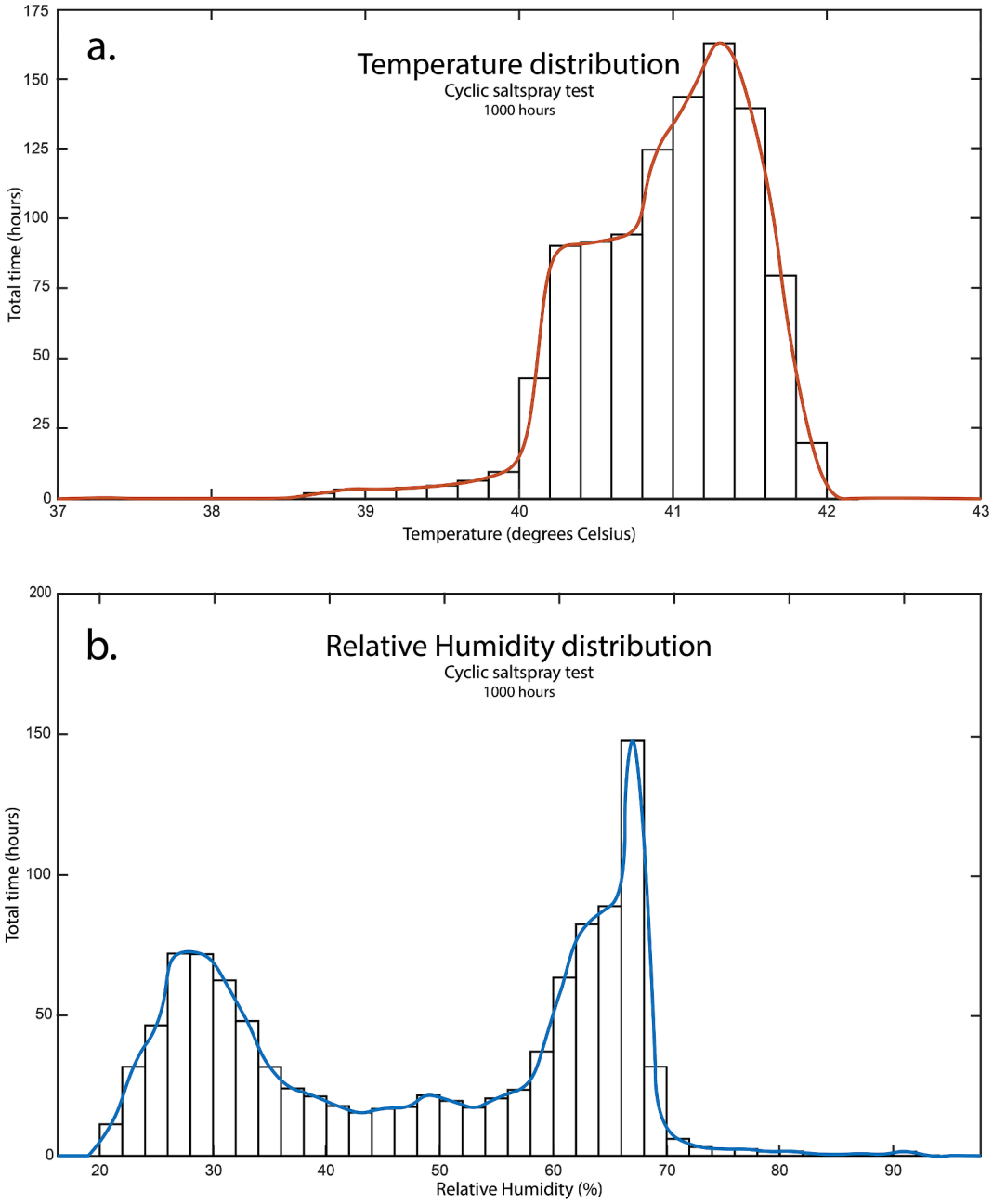

Fig. 3. Environmental conditions during the cyclic salt spray test: (a) temperature and (b) relative humidity variation throughout the test.

Further analysis of the environmental data reveals a difference in RH fluctuations during the day-night cycle. In winter, the average RH fluctuates between 75 % and 93 %, while in summer, it changes between 70 % and 86 %. This indicates that, on average, the RH exceeds 80 % for more hours per day in winter and primarily occurring at night. During winter season, the RH exceeds 80 % more than twice as often as in summer.

Throughout the entire exposure duration, the RH exceeded 80 % for 51 % of the time, totalling approximately 9000 h. Based on this data, it can be inferred that corrosion driven by TOW primarily occurs during winter nights, winter days and during summer nights. During these TOW periods, relatively low temperatures are observed, averaging 10 ± 14 °C, which slows down corrosion progression [29,33].

Another critical factor is the amount of RH transitions across the 80 % threshold, as previous studies indicate that corrosion is most likely to occur during these transition phases due to surface wetting and drying [33–36]. During these transitions, a thin electrolyte film forms on the surface as a result of the salt's hygroscopic properties [37]. The thickness of this film affects the salt concentration within the electrolyte, which, in turn, influences the corrosion rate [38]. Analysis revealed a total number of 1626 of these RH transitions over the exposure duration, corresponding to approximately 813 humidity cycles.

3.1.2. Cyclic salt spray test (CSST)

Environmental data recorded during the CSST include air temperature and RH, were logged using Luna sensors and are presented in Fig. 3. The dataset clearly shows distinct cycles of high humidity followed by dry-off phases. Over the course of the test, the specimens experienced approximately 500 humidity cycles.

The salt spray phase, identifiable as a peak around 68 % RH in the graph, was followed by high humidity and dry-off periods. The test maintained a consistent high temperature compared to outdoor exposure environments, aligning with CSST parameters. Specifically, this test temperature, which was 30 °C higher than outdoor exposure temperatures, resulted in an almost 8-fold increase in the corrosion rate, based on the Arrhenius equation ($k = A \bullet e^{\frac{-E_a}{RT}}$) (assuming an activation energy (E_a) of approximately 50 kJ/mol for AA2024) [33,39].

Further analysis of the RH data indicated that the TOW, defined in this test as RH ≥55 %, accounted for approximately 250 out of the total 1000 test hours. This relatively low RH threshold was chosen based on supporting data from solution resistance and polarization resistance measurements. Luna sensors recorded a drop in solution resistance when the surface became wet as well as a corresponding decrease in polarization resistance during active corrosion events, as shown in Fig. 4.

These results align with previous studies showing that dissolved salts on surfaces lower the TOW threshold by several tens of percents due to the adsorption of water vapour by saline solutions [40,41]. These findings highlight the importance of accounting for the effects of surface salt contamination when interpreting TOW and corrosion behaviour.

3.1.3. Flight test

During the flight test period, the aircraft were primarily parked in shelters, which significantly influenced the environmental exposure of the panels during the in-service exposure. To assess the influence of parking location, Luna sensors were installed to monitor environmental conditions. The environmental data collected in shelters were compared to local airfield conditions logged by the KNMI to better understand the environmental factors influencing degradation experienced during service.

Fig. 5 shows that shelter conditions essentially moderated the temperature fluctuations. In shelters, temperatures averaged in winter around 10 ± 5 °C and in summer around 21 ± 8 °C. In contrast, outdoor winter and summer temperatures were 7 ± 13 °C and

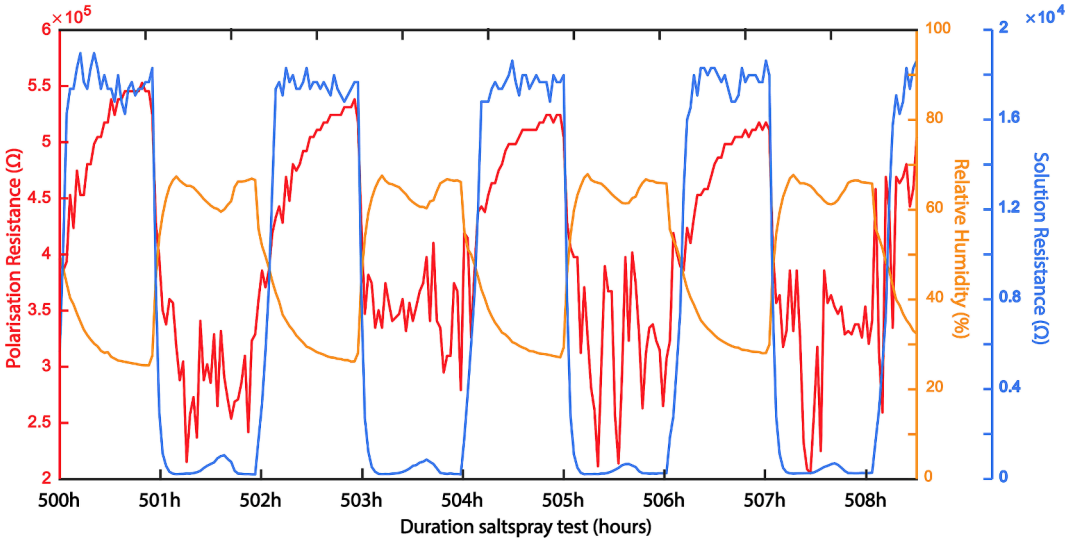

Fig. 4. Relative humidity, solution resistance and polarization resistance between 500 and 508 h during CSST.

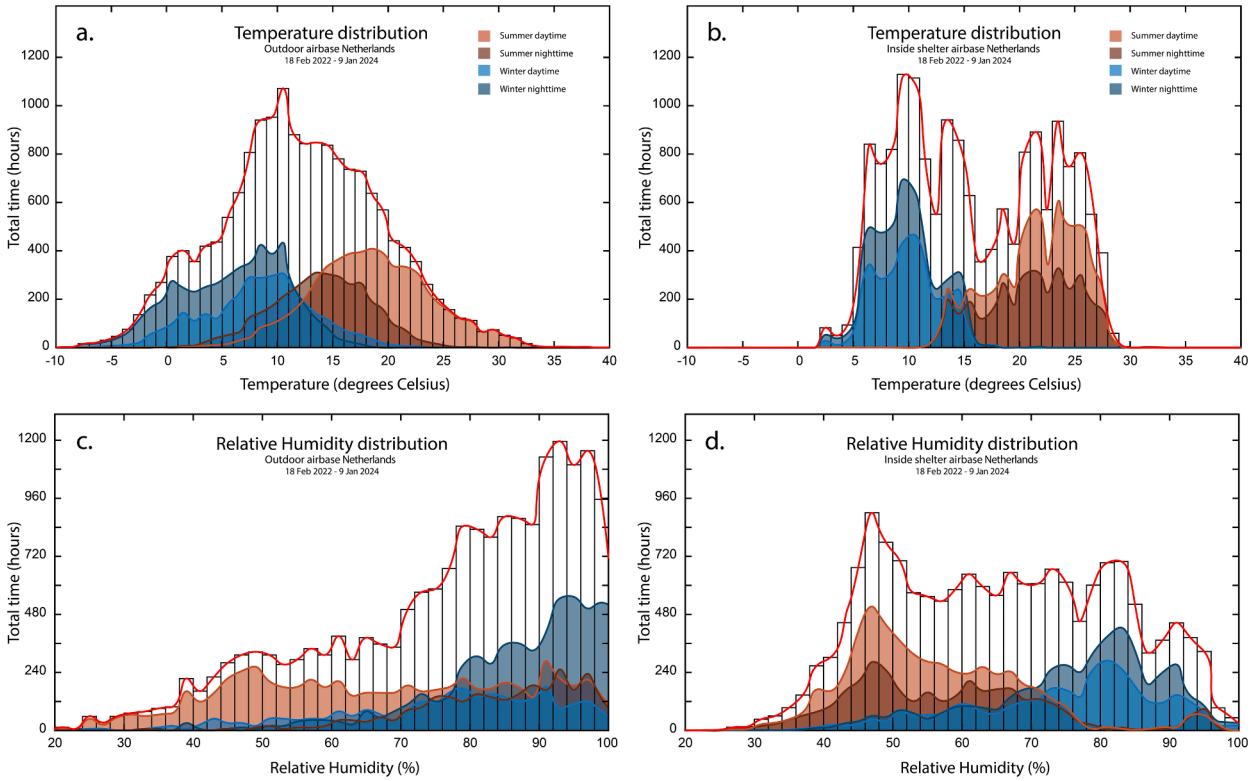

Fig. 5. Comparison of Environmental Conditions Between Outdoor Airfield and Shelter: (a) Temperature Distribution at the Airfield; (b) Temperature Distribution in the Shelter; (c) Relative Humidity Variation at the Airfield and (d) Relative Humidity Variation in the Shelter, presented over the exposure period, categorized by season and day vs. nighttime conditions.

17 ± 13 °C, respectively. This stabilization is attributed to the thermal properties of concrete shelters, absorbing and releasing heat, thereby regulating internal temperatures. From a corrosion perspective, the higher average temperatures in shelters would increase the corrosion rate by approximately 30 %, according to the Arrhenius equation (1) [33,39].

However, the moderation on temperature also affects the RH. Inside shelters, the RH exceeded the TOW threshold (RH ≥ 80 %) for only 15 % of the total time, as compared to over 50 % for outdoor environments. This difference was most pronounced during winter and nighttime, when temperatures outside were lower, leading to higher outdoor RH levels. The reduced TOW inside shelters is expected to result in approximately three times less corrosion as compared to outdoor conditions. When considering both temperature and RH effects, the corrosion rate inside a shelter is reduced by approximately 60 % compared to outdoor exposure.

RH fluctuations were also analyzed to estimate the number of humidity cycles in shelters during the test period. In 690 days, the RH crossed the 80 % threshold (up or down) 206 times in shelters, compared to 1343 times in outdoor environments, approx. 6.5 times less frequent. During the 2.5-year test period, aircraft parked in shelters experienced an estimated 272 RH transitions, equivalent to 136 complete cycles.

Flight conditions added additional environmental variability. The aircraft logged an average of 275 flight hours during the test period, with each 1.5 flight hours corresponding, on average, to one flight cycle (take-off, cruise and landing). During flights, the temperature decreases during ascent, stabilizes during cruise and increases again during descent and after landing. The low temperature at high altitude leads to condensation on the cold aircraft materials during landing. This condensation gradually evaporates as the material equilibrates with the ambient conditions.

These flight cycles significantly impact corrosion. Over the 2.5-year test period, each aircraft experienced an average of 183 flight cycles. Combined with shelter data, this corresponds to 319 RH cycles per aircraft over the course of the test period.

3.2. Visual observations

3.2.1. Outdoor exposure

The outdoor exposure panels were visually inspected every three months throughout the testing period. Observations revealed that the most significant corrosion progression occurred around the stainless-steel rivets. Fig. 6 provides an overview of the test panels, including detailed images that illustrate corrosion propagation around these rivets.

In addition, the structural coatings exhibited noticeable discoloration relatively early in the outdoor exposure period. This discoloration is likely due to UV radiation from sunlight. However, as structural aircraft components are typically not exposed to direct

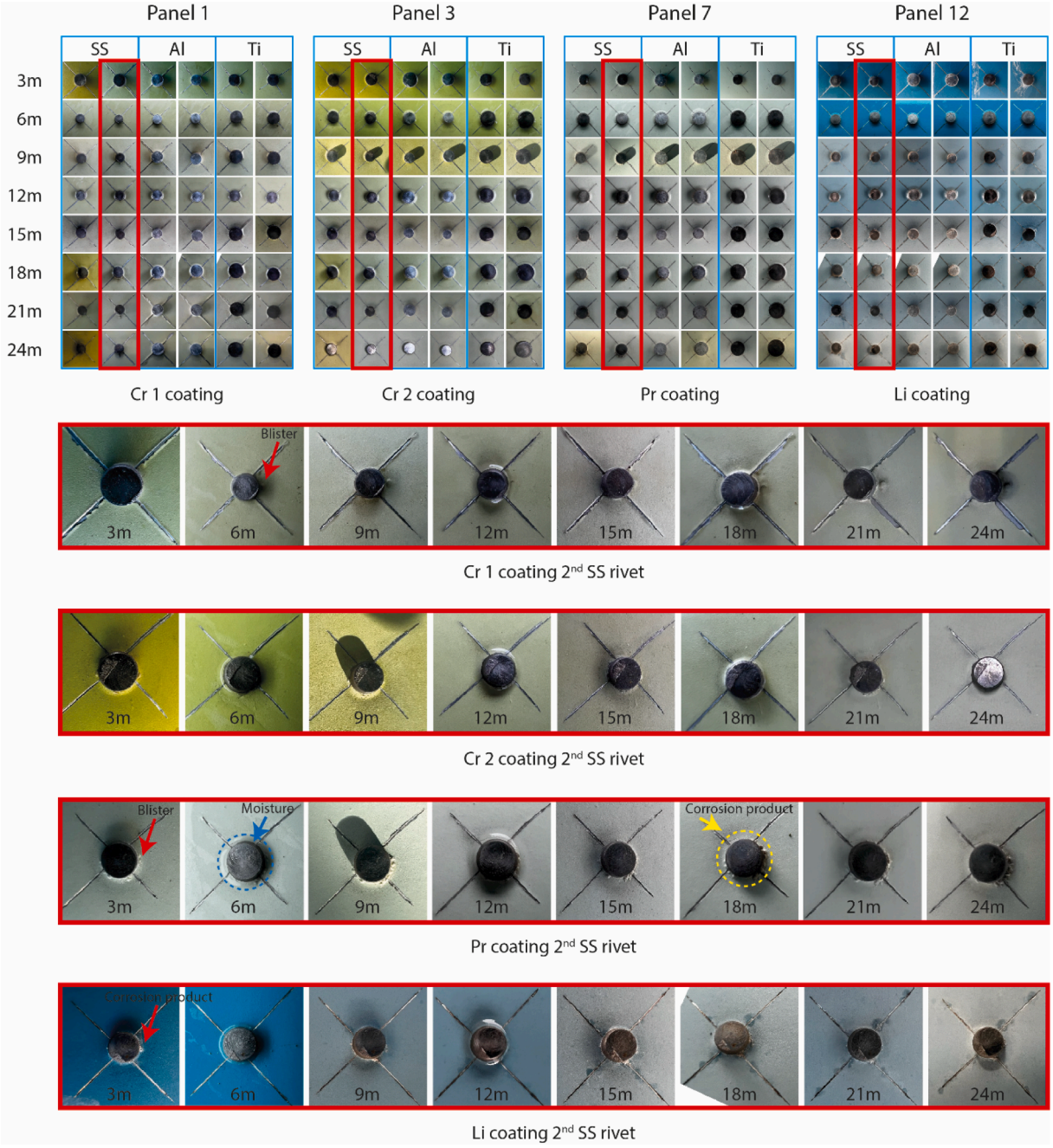

Fig. 6. Visual inspection results of outdoor exposure test panels with detailed images showing corrosion progression over time around X-scribed stainless-steel rivets for chromium, praseodymium and lithium coating systems.

sunlight, this degradation factor is less relevant for in-service applications, and results related to radiation damage may not directly correlate to operational conditions and performance.

The chromate-1 system exhibited coating failure during exposure. Blistering first appeared around the stainless-steel rivets after six months and continued to expand over time, though at a slower rate compared to the praseodymium system. Additionally, adhesion failure occurred, causing the coating to detach from the substrate.

In contrast, the chromate-2 system demonstrated exceptional performance. Even after two years of outdoor exposure, no signs of corrosion or coating degradation were observed, including around stainless-steel rivets, where other systems had failed early.

The praseodymium system showed blistering around stainless-steel rivets within the first three months of exposure. These blisters expanded over time. Similar blister formation was observed around titanium rivets after three months, though these were smaller and

grew at a slower rate. However, no visual corrosion or blistering was detected around aluminium rivets or inside the scribes without rivets.

The lithium-based system exhibited a distinctly different behaviour. No blisters were observed, but corrosion products formed on the coating surface. Corrosion first became visible after three months, particularly around stainless-steel rivets. Minor corrosion products were also detected around titanium rivets, though to a lesser extent. This corrosion progressed steadily throughout the exposure period. Notably, no corrosion or blistering was observed around aluminium rivets or in scribed areas without rivets.

3.2.2. Cyclic salt spray test (CSST)

Given the rapid corrosion progression observed around stainless-steel rivets, the analysis of CSST panels focused primarily on these areas. Fig. 7 highlights the corrosion behaviour around stainless-steel rivets after 1000 h of CSST. During the test, the formation of a salt crust obscured corrosion growth around individual rivets. Residual salt crusts can still be seen on the rivets of the lithium and chromate-2 systems in Fig. 7.

The chromate-1 system exhibited coating failure after the CSST, which appeared as adhesion loss. Adhesion loss was observed around all rivet types, as well as in the scribe regions without rivets. No visible corrosion was detected.

In contrast, the chromate-2 system demonstrated no degradation or corrosion after the CSST, not even in areas surrounding the stainless-steel rivets.

The praseodymium system exhibited prominent blistering around the stainless-steel rivets. These blisters appeared differently from those observed during the outdoor exposure test. This variation warrants further investigation and will be explored in greater detail following the microscopic analysis.

For the lithium system, some corrosion product formation was observed on the coating surface around the stainless-steel rivets, but no visible corrosion was observed in the scribe areas or around other rivets.

3.2.3. Flight test

Quarterly inspections during the flight test revealed no signs of corrosion or visible degradation of any of the tested coating systems. This remained consistent throughout the entire test period. Fig. 8 clearly shows the absence of corrosion progression during the flight test.

3.3. Microscopic analysis

In order to gain deeper insights into corrosion inhibition, regions of interest identified through visual inspection were further analyzed using SEM and EDX. The analysis focused initially on evaluating the protection layer and corrosion products within the scribe. Furthermore, the inhibition behaviour of the coating systems in the vicinity of stainless-steel fasteners was assessed. The development and progression of corrosion in lap-joints surrounding these fasteners are also addressed.

3.3.1. Corrosion in scribes

3.3.1.1. Outdoor exposure. Fig. 9 presents cross-sectional and top-down views of the scribe for different coating systems after outdoor exposure. EDX-maps of the top-down views were generated to provide elemental information about the corrosion products.

Leaching of inhibitors from the coatings was observed in all coating systems, visible as a depletion front indicated by red lines in the cross-sections in Fig. 9. For all coatings, a uniform oxide layer was identified in the scribe. This layer measured approximately 2 μm thick in the chromate and praseodymium systems and around 1 μm thick in the lithium system. These oxide layers appear to have effectively protected the aluminium substrate during outdoor exposure.

For chromate-based systems, EDX analysis detected chromium within the scribe, which had likely leached from the coating. During the TOW, strontium chromate dissolves and migrates to the scribe where it deposits over cathodic intermetallic particles as a thin monolayer of chromium hydroxide. This monolayer adsorbs chromate, forming a protective oxide layer that inhibits corrosion [26,42–44]. On anodic areas, aluminium hydroxide forms, which also adsorbs chromate, contributing to the passivity of the oxide layer [26,42–44].

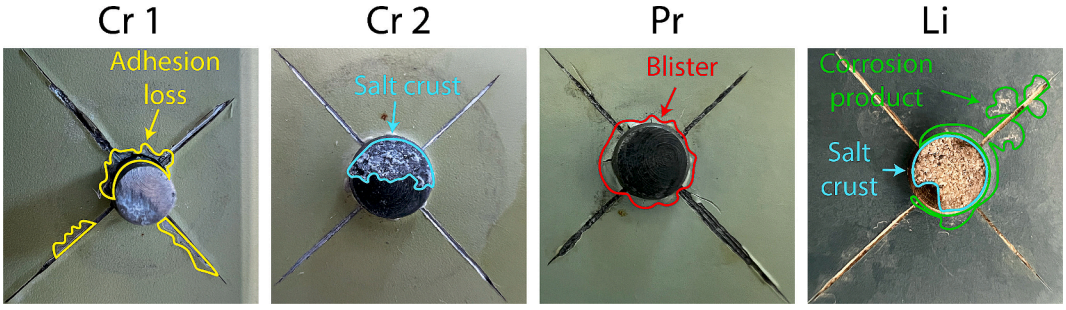

Fig. 7. Corrosion observed around X-scribed stainless-steel rivets after 1000 h of CSST for chromium, praseodymium and lithium coating systems.

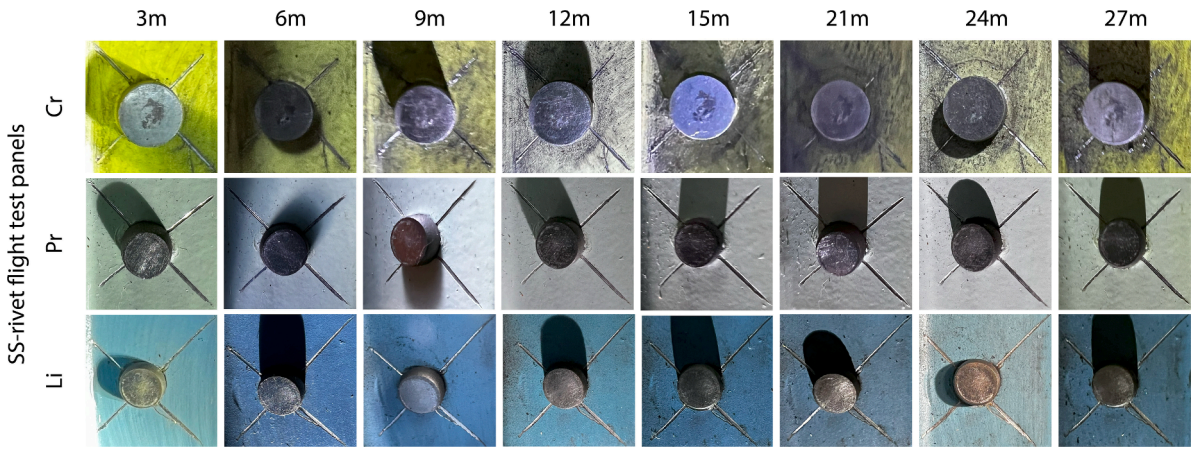

Fig. 8. Corrosion progression over time observed around X-scribed stainless-steel rivets during flight testing for chromium, praseodymium and lithium coating systems.

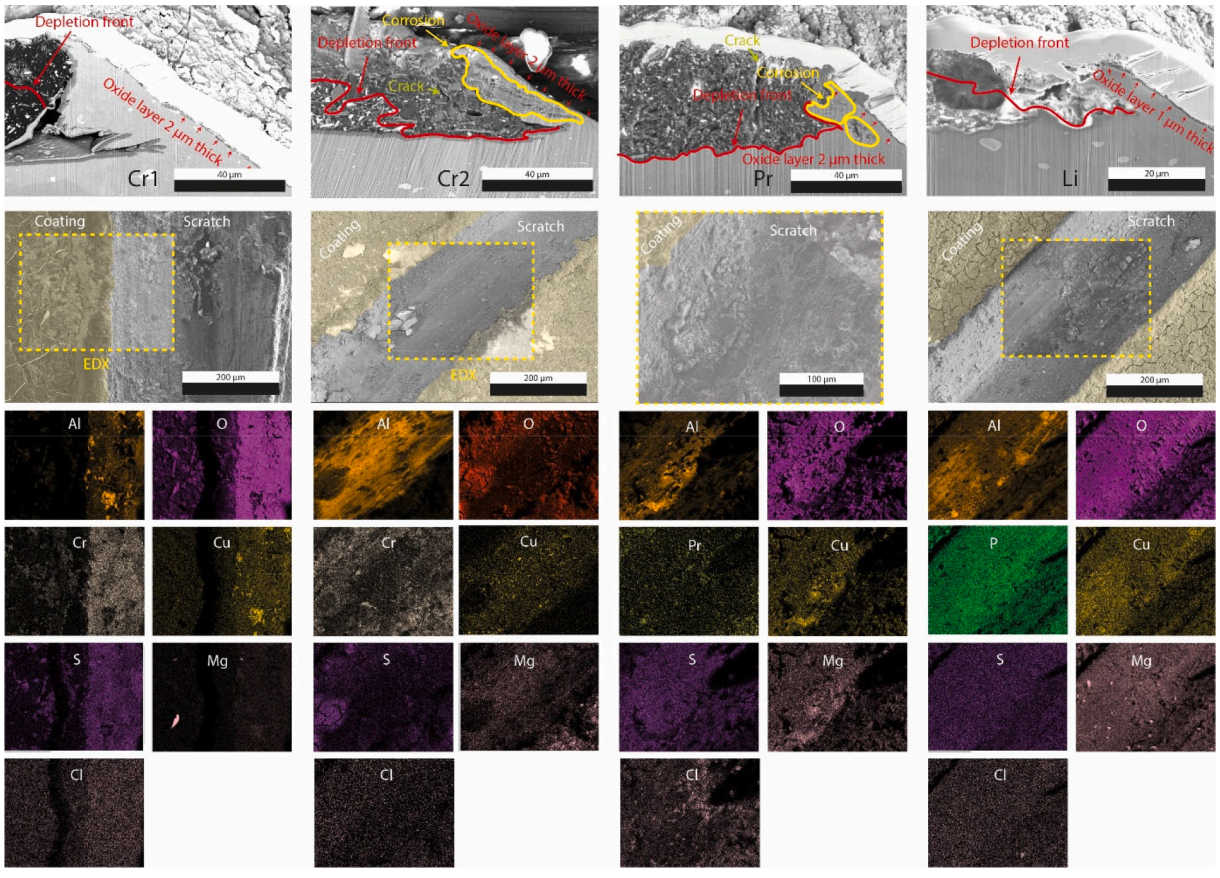

Fig. 9. SEM and EDX analysis of X-scribed area after outdoor exposure comparing chromium, praseodymium and lithium coating systems.

In the praseodymium system, EDX analysis detected praseodymium and sulphate in the scribe, which was leached from the coating as praseodymium oxide and calcium sulphate [12,45–48]. Praseodymium oxide dissolves in the moisture, migrates to the scribe and deposits as praseodymium hydroxide, praseodymium carbonate or as praseodymium (hydroxyl) carbonate [45,49]. These products inhibit corrosion by blocking cathodic intermetallic particles and reducing the oxygen reduction reaction (ORR). Furthermore, calcium sulphate enhances the leaching of praseodymium oxide and facilitates the formation of aluminium sulphate hydroxide on anodic areas. A synergistic effect on praseodymium gelation, as reported by Klomjit et al. [12], further improves corrosion inhibition.

The lithium system used lithium phosphate as its inhibitor. Leached lithium salts form Layered Double Hydroxides (LDH) on the aluminium substrate, first passivating anodic areas before extending towards cathodic intermetallic particles [50]. Although lithium is not detectible with EDX, phosphate was identified inside the scribe, which is consistent with the proposed passivation mechanism. Additionally, the oxide layer over cathodic areas was thinner than over anodic areas, aligning with the expected behaviour of LDH passivation.

Further analysis of the cross-sections revealed localized corrosion of the aluminium substrate in both the chromate-2 and praseodymium systems. This corrosion was confined to the burrs created during scribing, likely due to deformation, which made these areas more susceptible to corrosion.

In the chromate-1 system, insufficient pigment concentration was observed, likely due to inadequate mixing of the base component before adding the hardener during coating preparation. This led to reduced availability of the chromate inhibitor, which may explain the appearance of blisters after just six months of outdoor exposure. Additionally, adhesion issues were identified, with the coating failing to bond properly to the anodized oxide layer.

Regardless of the differences between the coating systems, the corrosion products in all scribes contained both sulphate and chloride, likely resulting from environmental exposure. The presence of these elements can be attributed to seawater, given the test site's coastal location approx. 5 km from the sea. Additionally, sulphate may also originate from jet fuel combustion, as the test site is an active airport [51,52].

Finally, cracks were observed in cross-sections of the chromate-2 and praseodymium coating systems. These cracks are likely occurred by UV radiation combined with the leaching of inhibitors during outdoor exposure [53].

3.3.1.2. Cyclic salt spray test (CSST). Fig. 10 presents cross-sectional and top-down views of the scribes in various coating systems after the CSST. EDX mapping of the top-down views was performed to provide elemental analysis of the corrosion products.

Similar to the outdoor exposure test, leaching of inhibitors was observed, indicated by depletion fronts in the cross-sections. In the chromate systems, oxide layers measuring 0.5–2 μm were identified within the scribe. These oxide layers provided effective protection in the chromate-2 system, preventing corrosion penetration into the substrate. By contrast, the chromate-1 system exhibited limited corrosion penetration, likely caused by insufficient inhibitor leaching which reduced its protective performance.

The lithium and praseodymium systems showed significant corrosion propagation, with damage extending deeply into the substrate. Corrosion products in these systems, as well as in the chromate-1 system, contained chloride, magnesium and sulphate, which

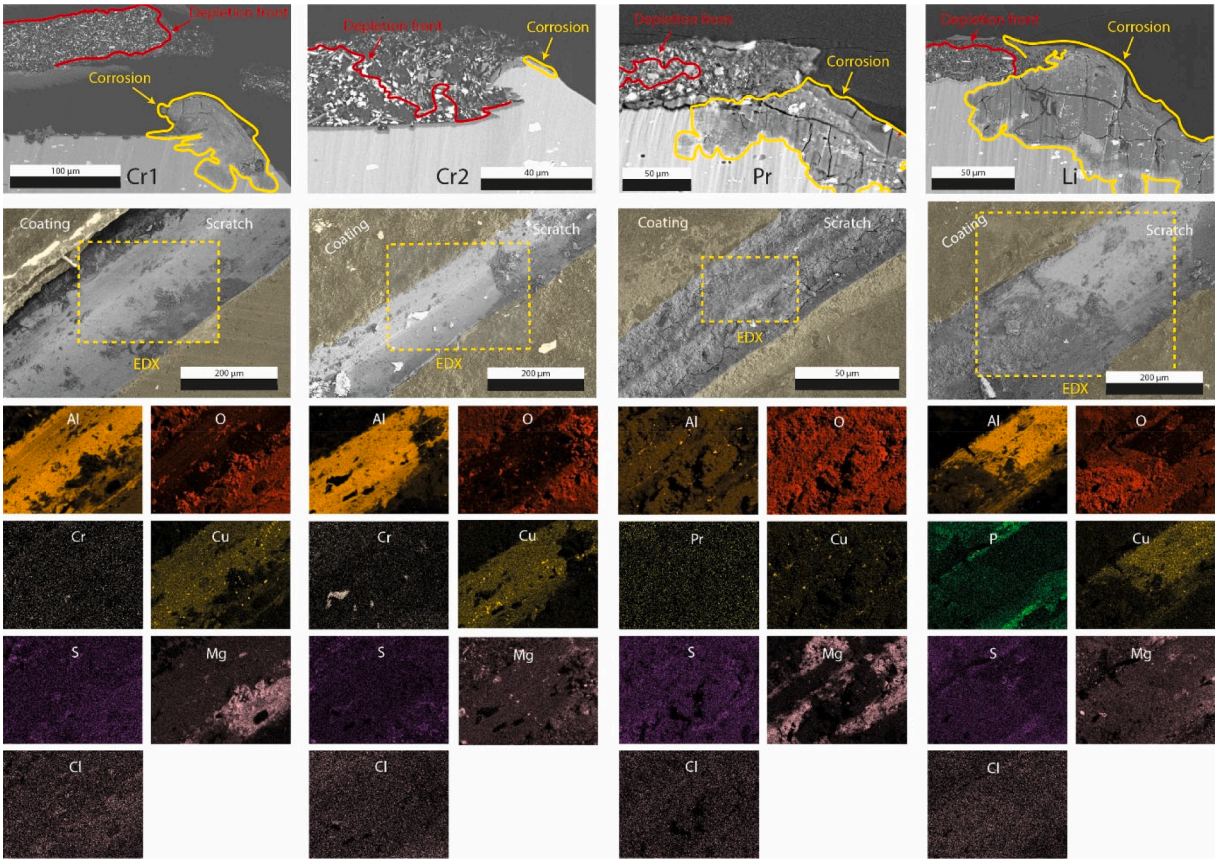

Fig. 10. SEM and EDX analysis of X-scribed area after CSST comparing chromium, praseodymium and lithium coating systems.

may originate from the artificial seawater solution used during the CSST. Chlorides increased the conductivity of the corrosion products, accelerating corrosion and thereby contributing to pitting [54,55]. Meanwhile, sulphates reacted with aluminium oxides or hydroxides to form hydrated aluminium sulphate, resulting in flaky corrosion products that exacerbated corrosion damage [51,52,56–58].

3.3.1.3. Flight test. Fig. 11 illustrates the cross-sectional and top-down views of the scribed coating systems after the flight test.

In addition to the visible leaching of inhibitors around the scribe, it is notable that corrosion within the scribe was observed only in the chromate-2 system. Unlike the praseodymium and lithium systems, no protective oxide layer was detected inside the scribe of the chromate-2 system.

A possible explanation for this lack of a protective oxide layer and the presence of corrosion in the chromate-2 system could be related to the panel's location on the aircraft. Specifically, the panel was installed in the hydraulic bay, where it was continuously exposed to hydraulic oil (Shell Fluid 41). The hydraulic oil likely caused the chromate to oxidize by reacting with organic components in the oil [59,60]. This reaction may have depleted the chromate, leaving insufficient quantities available to migrate into the scribe to provide corrosion protection.

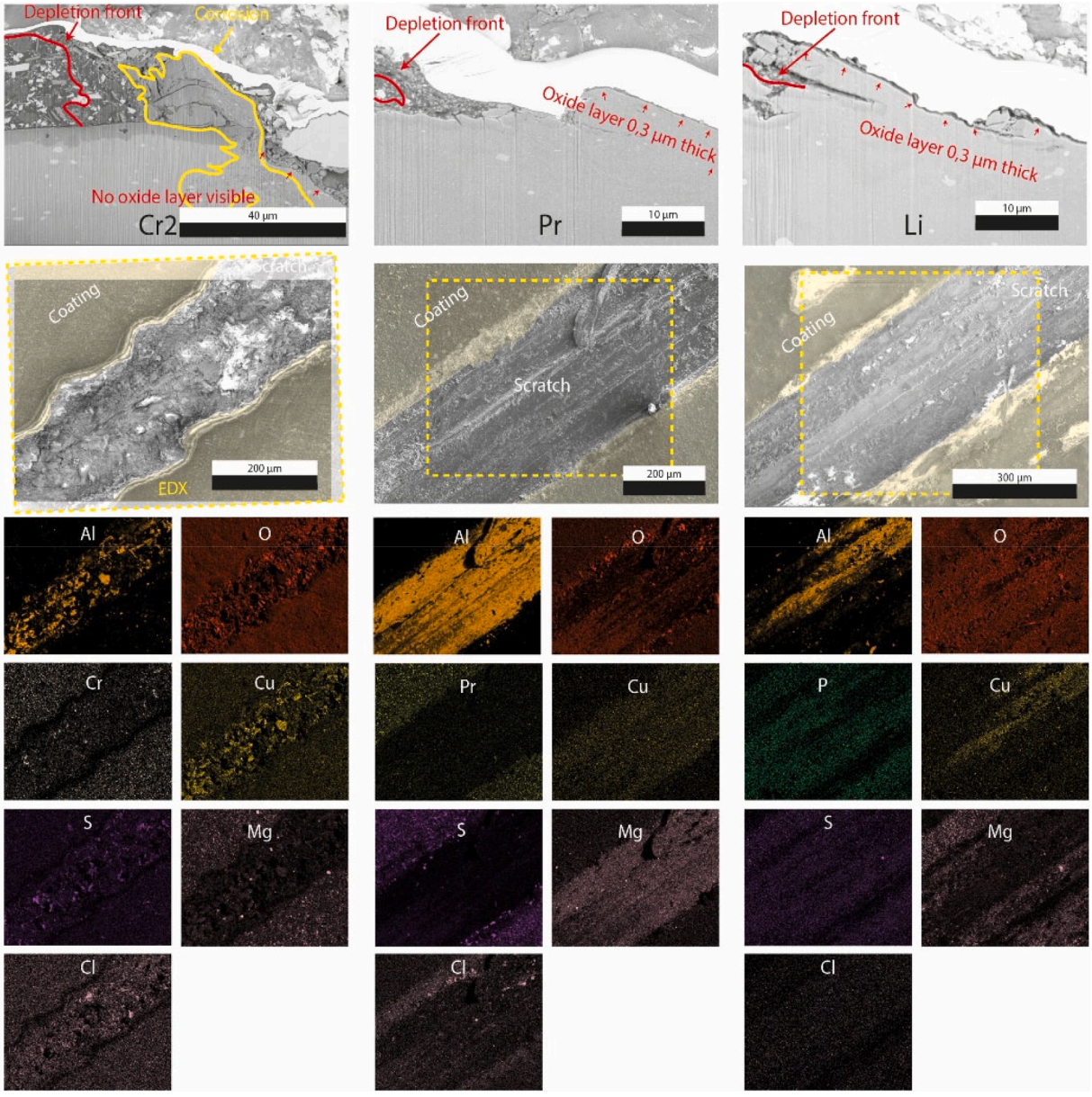

Fig. 11. SEM and EDX analysis of X-scribed area after flight test comparing chromium, praseodymium and lithium coating systems.

3.3.2. Galvanic corrosion around stainless-steel rivets

Corrosion around various types of fasteners, particularly around stainless-steel rivets, was analyzed during the different exposure tests to assess the performance of the coating systems.

3.3.2.1. Outdoor exposure. Figs. 12 and 13 show SEM cross-sectional analyses of stainless-steel rivets after outdoor exposure testing for the different coating systems.

For Al-Al coupled panels, as shown in Fig. 12, no corrosion was observed around the stainless-steel rivets in the chromate-based systems after outdoor exposure. SEM-EDX analysis identified a thin chromium- and nickel-rich oxide layer in the chromate-1 system. However, this layer was not clearly observed in the chromate-2 system, potentially due to deformation of the rivet during removal. Despite this, chromate appears to have protected the aluminium from corrosion, which is consistent with findings by Charles-Granville et al. [61] and Rafla et al. [62], who demonstrated that chromate provides cathodic passivation to stainless-steel when coupled with aluminium.

By contrast, Al-CFRP coupled panels, as shown in Fig. 13, corrosion was evident at the aluminium substrate around the stainless-steel rivets for both chromate systems. Chromate was unable to provide sufficient cathodic inhibition, likely because the large cathodic surface area of the CFRP panels exceeded the capacity of the inhibitors leaching from the coating to prevent corrosion.

Additionally, the interface between the coated aluminium panels and the adjacent layers (fibreglass or CFRP) was also examined to assess corrosion susceptibility of lap-joints. Fig. 14 provides an overview of these interfaces.

Interestingly, a certain degree of coating degradation was observed. Blistering was observed in the chromate-1 system at the fiberglass- as well as the CFRP side and in the chromate-2 system where it was in contact with the CFRP. By contrast, the chromate-free systems showed no coating degradation. This lack of degradation is likely caused by the use of advanced coating polymers, such as polyurethanes, which provide better moisture barriers as compared to traditional coatings based on epoxy polyamides [63,64].

The blistering observed in the chromate-1 system on the fiberglass side likely originated from direct contact of the fastener with CFRP and aluminium. This direct contact may have created localized corrosion leading to blistering. However, this corrosion process could also have been initiated by direct contact between the CFRP and the aluminium alloy, caused by the drilling process of CFRP materials [65].

These findings underscore the critical importance of selecting appropriate coatings for lap-joints involving dissimilar materials to prevent corrosion damage. In scenarios characterized by large potential differences and extensive cathodic areas where dissimilar

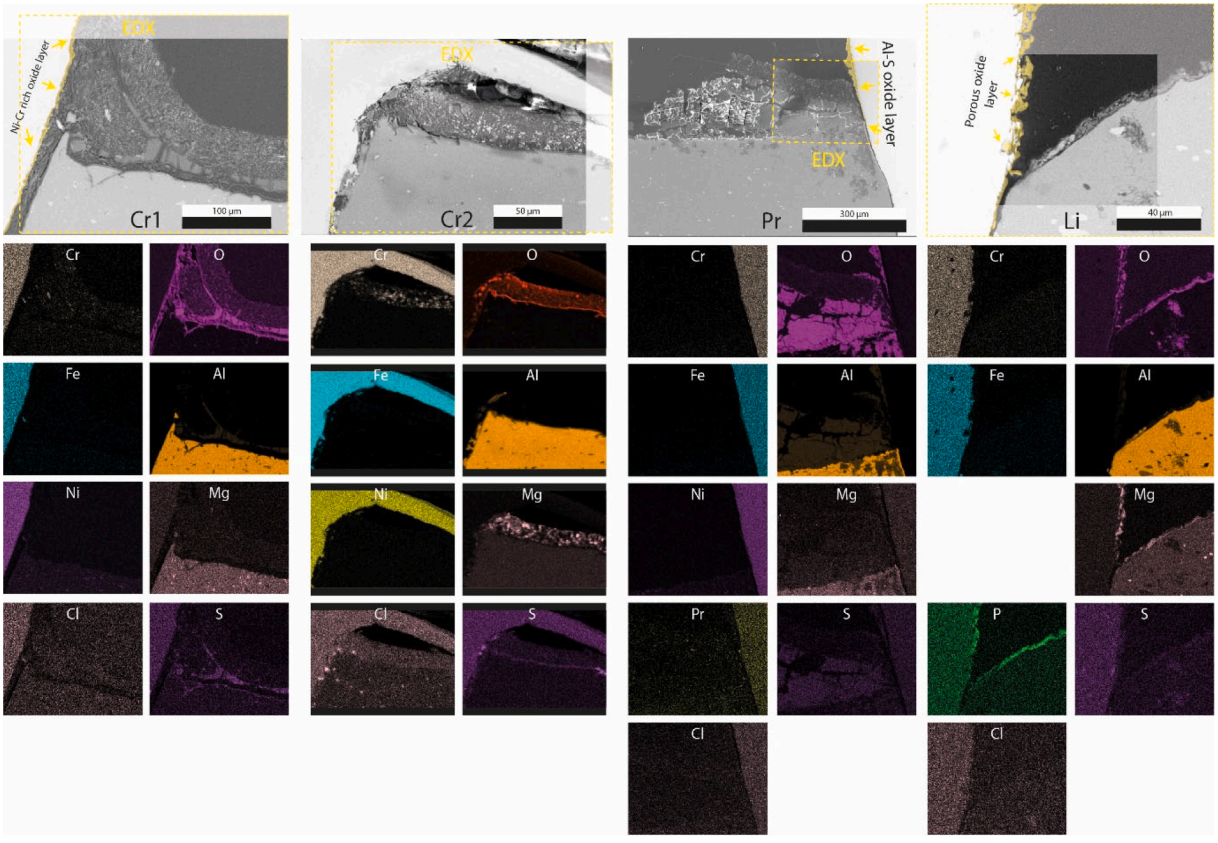

Fig. 12. SEM and EDX analysis of stainless-steel rivet cross-section after outdoor exposure comparing chromium, praseodymium and lithium coating systems (Al-Al coupled panel).

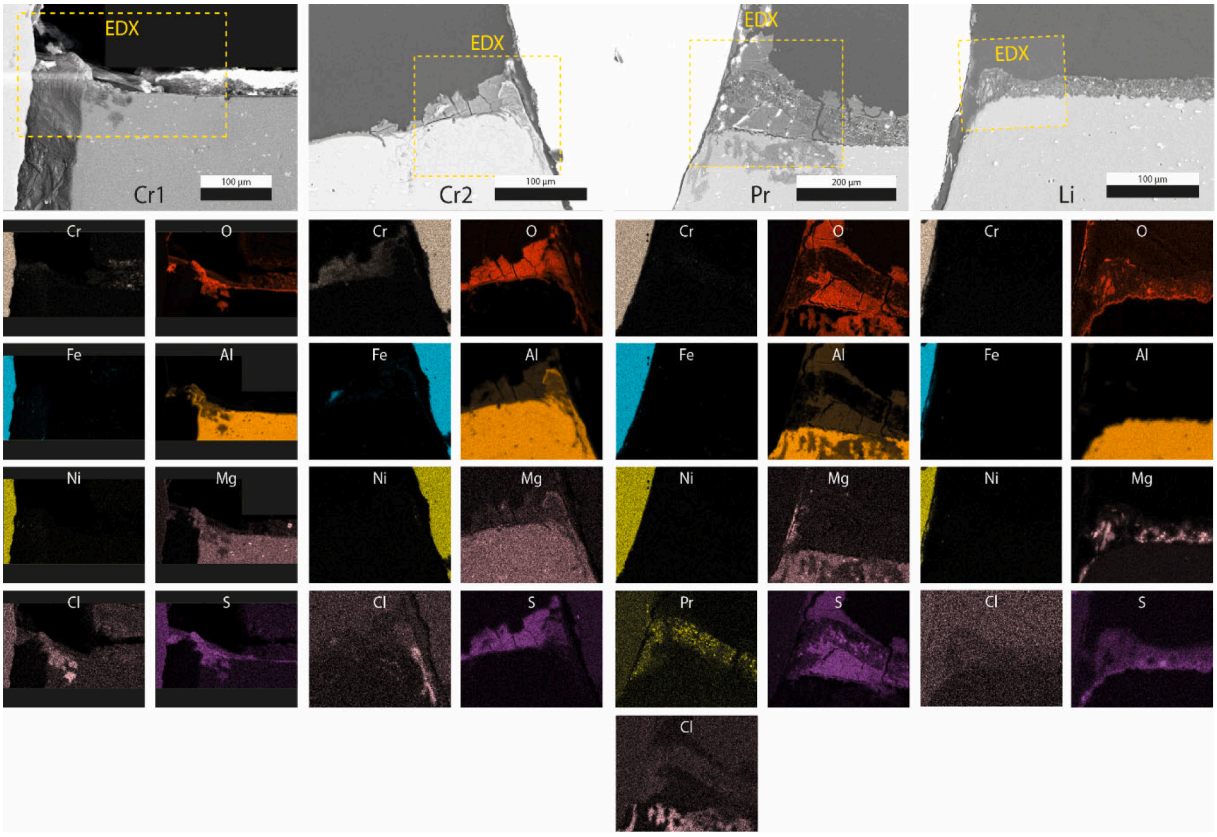

Fig. 13. SEM and EDX analysis of stainless-steel rivet cross-section after outdoor exposure comparing chromium, praseodymium and lithium coating systems (Al-CFRP coupled panel).

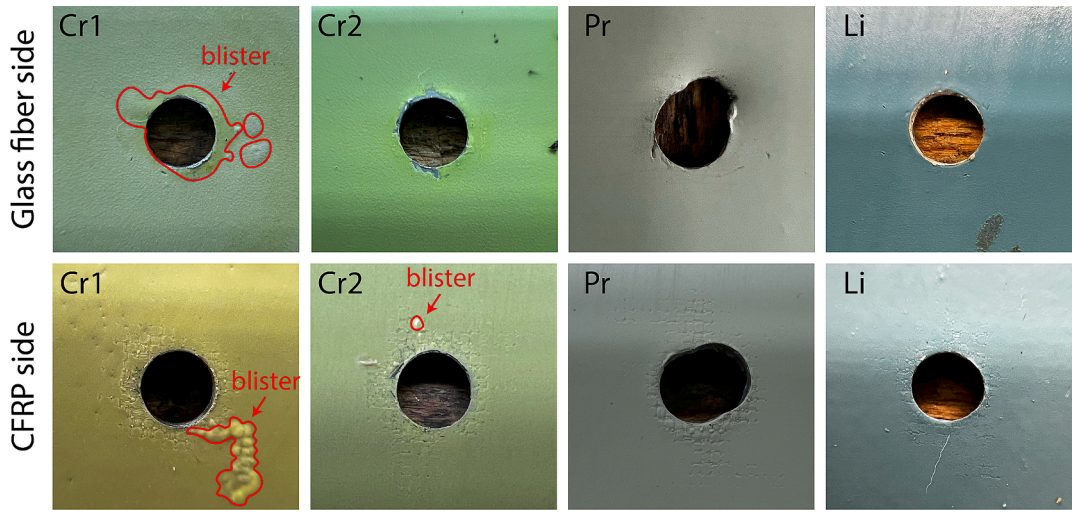

Fig. 14. Overview of lap-joint facing areas around stainless-steel rivets between CFRP and aluminium panels with different coating systems after outdoor exposure.

material coupling occurs, active corrosion protection provided by conventional coating systems proves to be of limited effectiveness. Instead, coatings or sealants with superior barrier properties should be employed to ensure robust corrosion protection in these areas, as also supported by van Es et al. [66].

3.3.2.2. Cyclic salt spray test (CSST). After the CSST, all coating systems exhibited corrosion around galvanically coupled stainless-steel rivets, as shown in Fig. 15. The chromate-1 and lithium systems showed more severe degradation as compared to outdoor exposure, while the praseodymium system showed less. This variation suggests that CSST creates different corrosion conditions than those observed during outdoor exposure.

A distinct difference between the CSST and outdoor exposure tests was also observed inside the lap-joints, as shown in Fig. 16. Corrosion in the lap-joints during the CSST progressed more slowly than in outdoor exposure tests. Coating failure in the CSST test was only observed in the chromate-1 system, specifically on a panel coupled with fibreglass.

These findings highlight the varying corrosion mechanisms between the CSST and outdoor exposure, emphasizing the need for complementary tests to assess coating performance comprehensively.

3.3.2.3. Flight test. The flight test panel configuration did not include any panels where CFRP material was coupled with aluminium. Consequently, the corrosion conditions were less severe. Indeed, no corrosion was detected around the rivets in any of the coating systems after the flight test, as shown in Fig. 17.

3.4. Differences in blister formation around stainless-steel rivets under various exposure conditions

Blister formation around rivets varied across different exposure conditions. Notably, more blisters formed after outdoor exposure compared to CSST, whereas no blisters were observed around rivets following flight testing. Additionally, differences in blister formation were observed across the various coating systems. The praseodymium-based coating exhibited the most severe blistering, while minimal blistering was observed at the chromate-based systems and no blistering occurred in the lithium-based coatings. This section first explains the differences in blister formation across the various exposure conditions and then explores the variations observed between the different coating systems.

3.4.1. Blister formation across various exposure conditions

Microscopic analysis revealed significant degradation of the coatings during outdoor exposure, likely due to UV radiation combined with the leaching of inhibitors due to rain. This degradation resulted in cracks extending to the substrate, as shown in Fig. 9. These findings align with studies showing that UV-induced photo-oxidation and polymer bond scission can promote cracking, allowing moisture ingress and further degradation of coating integrity [67–69]. In addition to this deterioration, coatings exposed to outdoor

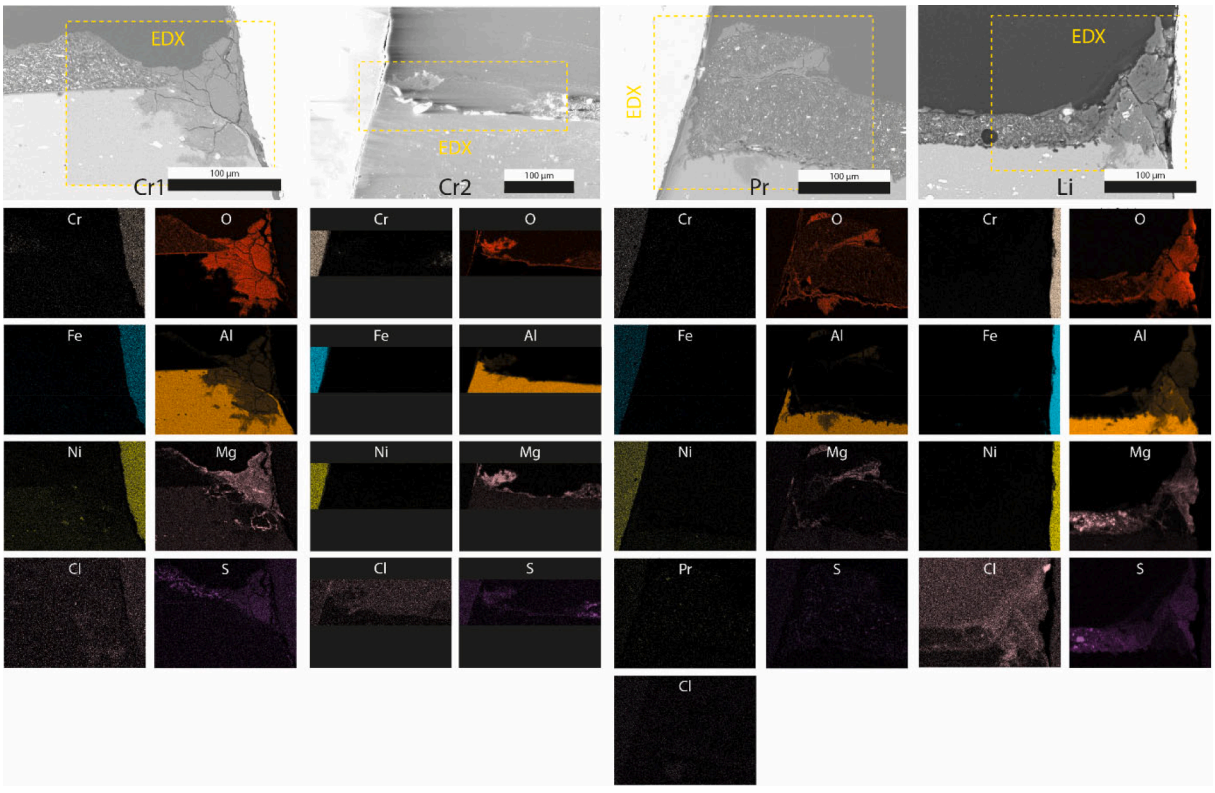

Fig. 15. SEM and EDX analysis of stainless-steel rivet cross-section after CSST comparing chromium, praseodymium and lithium coating systems (Al-CFRP coupled panel).

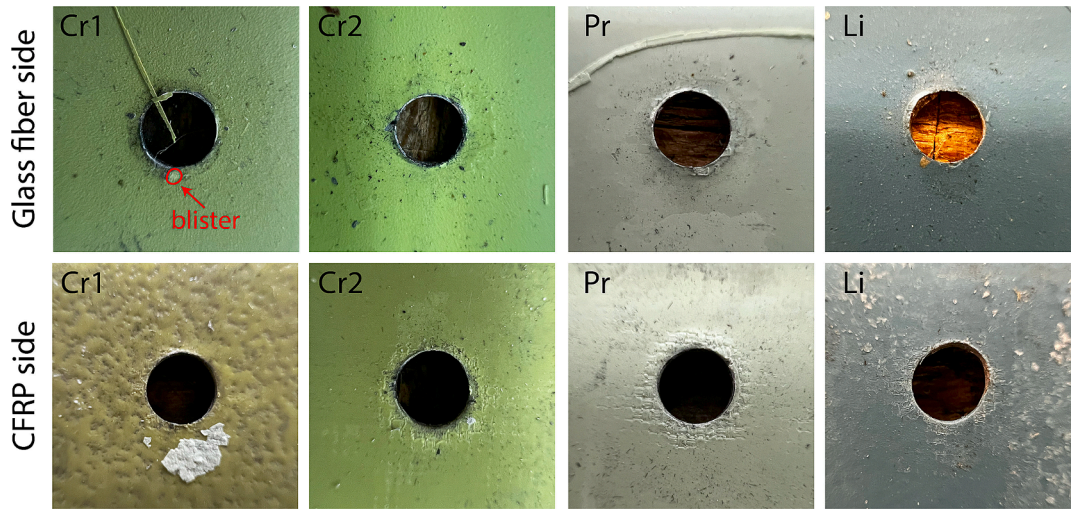

Fig. 16. Overview of lap-joint facing areas around stainless-steel rivets between CFRP and aluminium panels comparing chromium, praseodymium and lithium coating systems after CSST.

conditions were subjected to greater electrolyte exposure. Environmental parameter analysis showed that during outdoor exposure, RH exceeded 80 % for 9651 h, whereas in the salt spray chamber, RH remained above the threshold for only 500 h. Extended periods of high humidity have been associated with enhanced capillary action at coating defects, which traps moisture and accelerates localized corrosion processes [70].

Furthermore, visual analysis indicated that the ring of deposited corrosion products around rivets in outdoor exposure panels was larger than that in CSST panels, as shown in Figs. 6 and 7. This suggests that more electrolyte accumulated around rivets during outdoor exposure compared to CSST.

Based on these findings, Fig. 18 presents a schematic representation illustrating the different corrosion mechanisms that may lead to varying observations under different exposure conditions. During outdoor exposure, moisture accumulated between the rivet and the substrate, facilitated by condensation and/or rainfall. This moisture, combined with the galvanic potential difference between the rivet and the aluminium substrate, initiated localized corrosion of the aluminium, as illustrated in Fig. 18(1a) [71]. Capillary action likely retained moisture around the rivet, further promoting corrosion beneath the cracks in the coating. The formation of aluminium hydroxide led to acidification of the electrolyte underneath the coating, which degraded the polymer bonds and weakened coating adhesion [72,73]. As corrosion products expanded beneath the coating, osmotic pressure, driven by the ion concentration gradient in the electrolyte above and below the coating, caused delamination and blister formation, as depicted in Fig. 18(2a) [74].

By contrast, the corrosion mechanism during the CSST appeared different, as UV-induced cracking of the polymer matrix did not occur. The intact coating acted as a barrier, preventing the electrolyte from directly reaching the substrate (Figs. 18, 1b). As a result, the blistering observed during the CSST was primarily attributed to galvanic corrosion originating from the stainless-steel rivets, as shown in Fig. 18(2b). This aligns with literature highlighting that stainless-steel fasteners can create local galvanic cells in chloride-rich conditions, causing small, localized blistering [75].

Blisters were also observed around titanium rivets in the CSST panels, but these were smaller than those seen around stainless-steel. The aluminium rivets and scribed areas without fasteners appeared unaffected by corrosion or blistering. This further indicates that the corrosion process was primarily driven by galvanic interaction as described by MIL-STD-899 [71,75].

3.4.2. Blister formation across various coating systems

In addition to variations in blister formation between different exposure conditions, distinct differences were observed among the various coating systems. These differences can be attributed to the effects of different corrosion inhibitors as well as to the variations in polymer matrices used in each system. This section first examines the chromate-based coatings, followed by the praseodymium and lithium-based systems.

3.4.2.1. Chromate-Based systems. Blister formation in the chromate-1 system was minimal, with only slight blistering observed after six months of outdoor exposure. By contrast, the chromate-2 system exhibited no blistering under the same conditions. The reduced blister formation in these systems is likely due to the presence of a protective oxide layer around the rivets, as observed in Fig. 12. This oxide layer may have significantly suppressed the ORR on the cathodic side, leading to a reduced formation of hydroxide ions (OH^-) [61,62]. The lower OH^- concentration likely inhibited aluminium hydroxide formation, preventing significant pH shifts in the electrolyte. As a result, polymer degradation due to acidification was minimized, preserving the coating's adhesion to the substrate [72,73]. Additionally, the suppression of electrochemical reactions may have limited ion concentration fluctuations, thereby reducing osmotic pressure differentials—a primary driver of blister formation [72]. These findings suggest that chromate-based inhibitors play a

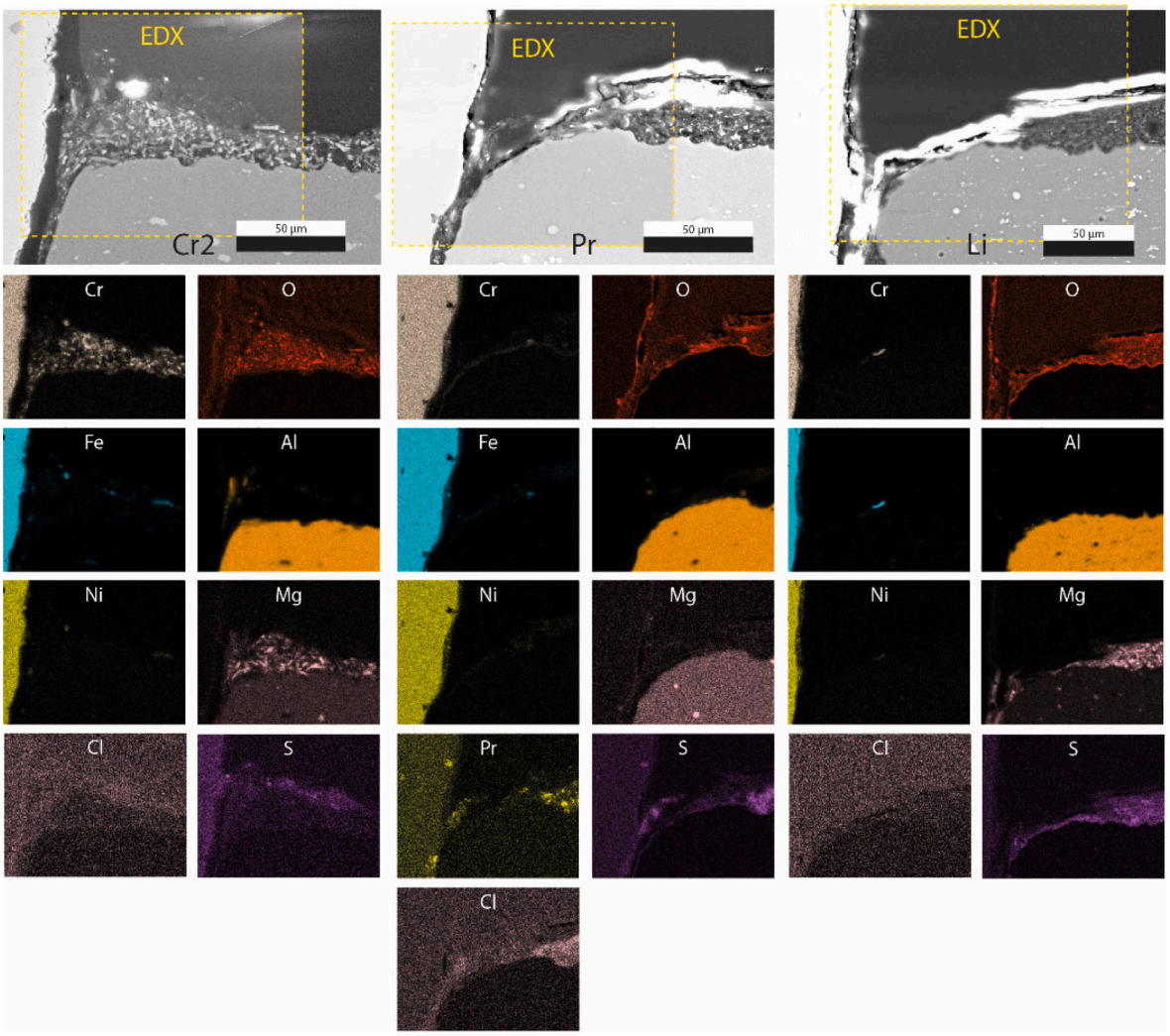

Fig. 17. SEM and EDX analysis of stainless-steel rivet cross-section after flight test comparing chromium, praseodymium and lithium coating systems (Al-stiffener and Al-coupled panel).

critical role in mitigating blistering by stabilizing both the chemical and electrochemical environment around rivets.

3.4.2.2. Praseodymium-Based system. In contrast, the praseodymium-based system exhibited severe blistering as early as the three-month inspection during outdoor exposure. Unlike the chromate coatings, no protective oxide layer was observed at the rivets in the praseodymium system (Fig. 12). This absence suggests that praseodymium was ineffective in suppressing the ORR, leading to more pronounced localized corrosion and subsequent blistering.

Apart from the inhibitor's inefficacy, the polymer matrix used in the praseodymium system may have contributed to the observed blister formation. Similar to chromate coatings, this system employs an epoxy polyamide matrix. The amide groups in the epoxy polyamide structure create polar sites, allowing water molecules to bind to the polymer network [76,77]. This enhances moisture uptake and reduces the overall hydrophobicity of the coating, which ranges between 60° and 80° contact angles [78]. Consequently, the greater hydrophilicity of the epoxy polyamide matrix, combined with the lack of effective ORR suppression by the praseodymium-based corrosion inhibitors, likely explains the extensive blistering observed in the praseodymium-based coating system.

3.4.2.3. Lithium-Based system. The lithium-based system showed no significant blister formation, similar to the chromate-2 system. However, as with the praseodymium coating, no protective oxide layer was observed at the rivets, suggesting that ORR inhibition was not achieved through lithium-based reactions. Lithium is known to form LDHs, which can create protective oxide films on the anodic site [50]. Nonetheless, given the significant potential difference between the stainless-steel rivets and the aluminium substrate and the concentration of corrosive anions like chlorides, this protective layer may be unstable and prone to breakdown, preventing the formation of a consistent, long-lasting barrier [11,79].

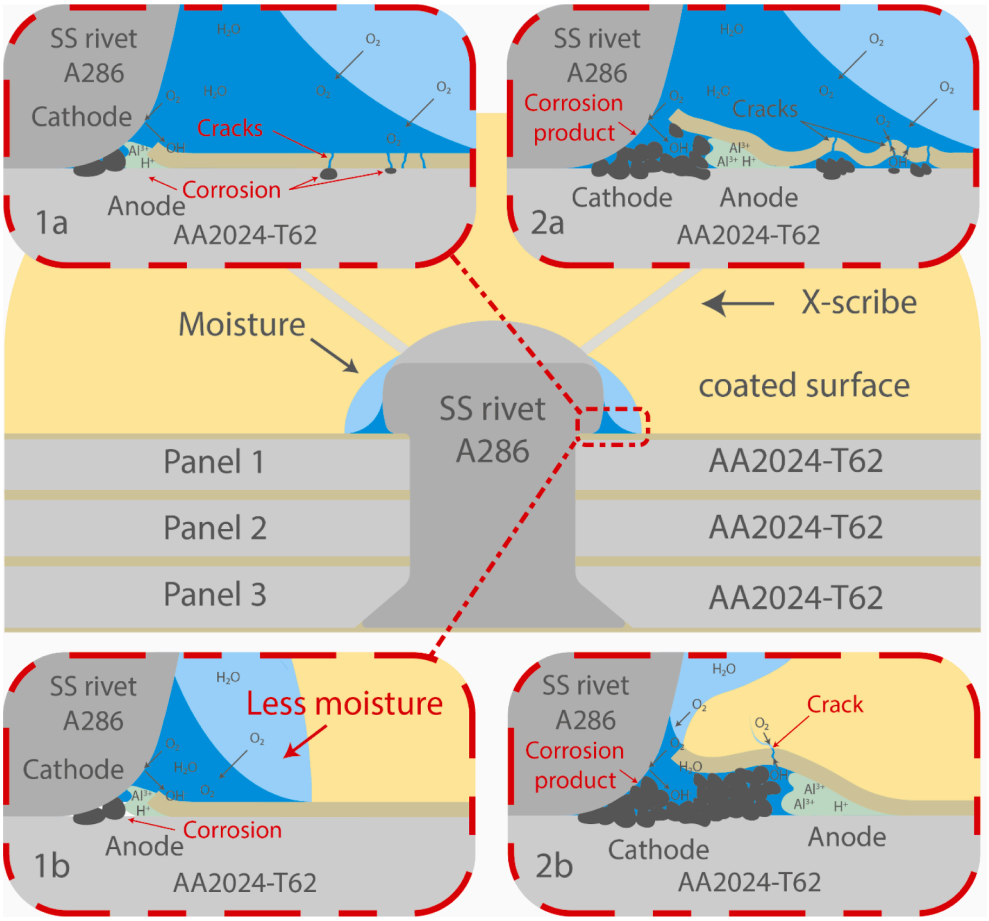

Fig. 18. Schematic representation of the corrosion mechanisms around stainless-steel rivets in the praseodymium coating system: (1a) and (2a) depict the proposed corrosion mechanisms during outdoor exposure, whereas (1b) and (2b) represent the proposed corrosion mechanisms during CSST.

The aliphatic segments in polyurethane reduce its overall polarity, thereby increasing its hydrophobicity. This leads to contact angles exceeding 80°, making polyurethane coatings less prone to moisture uptake than epoxy polyamide-based systems [80–82]. As a result, the higher hydrophobicity of polyurethane likely contributed to the lower blister formation observed in the lithium-based system [83].

The findings suggest that blister formation is influenced by both the type of corrosion inhibitor and the polymer matrix used in the coating system. Chromate-based coatings exhibit strong ORR suppression and protective oxide formation, resulting in minimal blistering. The praseodymium-based system lacks these protective mechanisms, leading to severe blistering due to increased hydrophilicity and ineffective ORR inhibition. The lithium-based system, despite its absence of a cathodic protective oxide layer, benefits from the hydrophobic properties of its polyurethane matrix, which helps to reduce water uptake and to mitigate blistering. Understanding these interactions is critical for the development of chromate-free corrosion protection solutions in aerospace applications.

3.5. Relationship between exposure environments and observed corrosion

This section explores the relationship between environmental exposure conditions, summarized in Table 2, and the observed corrosion behaviour.

As shown in Table 2, the TOW during a RH cycle averages at approx. 11 to 12 h for both outdoor exposure and flight testing. However, during the CSST, the TOW is significantly shorter, lasting only about 60 min per cycle. Furthermore, it should be noted that, if a coating fails and corrosion occurs during the TOW, the elevated test temperature of 40 °C in the CSST (as compared to 10 °C for the other tests) accelerates corrosion processes approximately by a factor of 8 [33,39].

Significant differences in saline exposure were also observed between the different environments. During the flight tests, no visible salt deposition was detected. For outdoor exposure, salt deposition was observed periodically. However, the panels were frequently washed by rain. By contrast, the CSST included a 15-minute salt spray every 2 h using an artificial sea salt solution, leading to the formation of a persistent salt crust on the test panels.

Table 2
Summary of corrosion-related environmental conditions during different exposure tests.

	Outdoor exposure	Cyclic salt spray test	Flight test
Avg. Temperature during TOW (°C)	10 ± 14	40 ± 3	10 ± 9
Total TOW (h)	9651	500	3904
RH-cycles	813	500	319

The impact of these environmental factors on corrosion failure mechanisms is reflected in the findings of the cross-sectional SEM analyses of the scribes, summarized in Table 3.

The results indicate that the corrosion behaviour observed during the CSST does not align with the behaviour observed after outdoor exposure or flight testing. For instance, during the CSST, the chromium-1, praseodymium and lithium coating systems showed rapid corrosion progression, whereas these remained protected or exhibited only minor corrosion in outdoor exposure and flight tests. Conversely, the protection of the chromate-2 system observed in the CSST did not align with the minor corrosion observed in outdoor and flight testing.

These discrepancies are likely caused by the variations in salt loading. The extreme salt crust formation during the CSST may activate different corrosion mechanisms as compared to the moderate salt deposition during outdoor exposure and the negligible salt loading during flight tests. Additionally, the shorter TOW per cycle in the CSST may have impeded corrosion, resulting in the observed differences.

Since the CSST exposure does not accurately reflect real-world conditions, the results from the outdoor exposure and flight tests are still promising. These suggest that alternative coatings developed to replace chromate can effectively protect damaged aluminium alloy AA2024-T62 substrates from corrosion under representative conditions. To further assess the suitability of these coatings for aluminium structural aircraft components, it is recommended to conduct similar tests on other alloys, such as AA7075-T6, or perform flight tests on non-critical parts to evaluate the protective behaviour of these alternative coating systems.

The comparison of metrological and climatological data with corrosion findings illustrates discrepancies among outdoor exposure, CSST and in-service conditions, revealing critical gaps in current artificial aging tests. This insight provides a framework for future research to optimize test parameters to improve the correlation between laboratory results and real-world performance. Furthermore, it is worth to reconsidering whether accelerating corrosion to the point of coating failure with visual detectability is necessary, as microscopic analysis—as demonstrated in this study—can effectively assess corrosion progression and evaluate the corrosion-preventive performance of different samples.

4. Conclusions

Based on the findings of this study, the following conclusions can be drawn:

i. **Accelerated testing methods need refinement for specific applications**; accelerated testing methods that replicate real-world corrosion processes and accurately predict the long-term performance of coating systems remain challenging. The CSST did not match with the results from outdoor exposure tests or flight tests. Even for chromate-containing coatings, the CSST was unable to predict which system would perform better in outdoor environments. This discrepancy is likely due to the varying corrosion mechanisms triggered by different environmental conditions, such as UV radiation. Therefore, it is crucial to refine testing conditions to match specific applications. Key adjustments required include:
   a. Salt deposition: The salt deposition in CSST-induced corrosion mechanisms is not observed under flight conditions;
   b. Variations in TOW: Extended periods of wetness result in different corrosion patterns than those observed during real-world service;
   c. UV radiation: Outdoor exposure accelerates inhibitor leaching and barrier degradation via UV radiation, a factor that internal structural components typically do not encounter during service.

ii. **Chromate-free coating systems based on praseodymium and lithium demonstrate promising active corrosion protection;** following outdoor exposure and flight testing, these coatings formed protective oxide layers in damaged areas, limiting further corrosion. While these performed well on AA2024-T62 alloys, further research is required to assess their performance on other alloys. Additional flight testing on non-critical parts could provide valuable insights into their long-term behaviour.

iii. **Chromate-free coating systems were less effective at preventing galvanic corrosion around stainless-steel fasteners**; in fact, even chromate-based systems failed to protect aluminium panels coupled with fasteners to CFRP. This highlights the

Table 3
Overview of SEM analysis of corrosion in cross-sectioned scribes.

Coating system	Outdoor exposure	Cyclic salt spray test	Flight test
Cr1	protection	corrosion > 50 μm	–
Cr2	protection, minor corrosion < 15 μm	protection	protection, minor corrosion < 30 μm
Pr	protection, minor corrosion < 15 μm	corrosion > 50 μm	protection
Li	protection	corrosion > 50 μm	protection

persistent challenge of ensuring robust corrosion protection in complex multi-material assemblies, emphasizing the need for continued research to develop more effective protection strategies.

iv. **Chromate-free coating systems outperformed traditional chromate-based coatings in lap-joint configurations where aluminium panels were coupled with CFRP;** this improved performance is likely due to advancements in the polymer matrix formulation, which enhance their barrier properties and prevent galvanic coupling more effectively. For these specific configurations, robust barrier coatings offer superior protection as compared to active protective coatings.

Based on these conclusions, this study recommends the following environmentally friendly preventive measures against corrosion for structural aircraft applications: to mitigate galvanic corrosion, isolation techniques that minimize electrochemical interactions between dissimilar materials should be adopted. In such cases, it is preferable to use highly crosslinked polymer coating systems with enhanced barrier properties to isolate materials, rather than relying on active corrosion protection. However, for aluminium components that are not coupled with different materials, coating systems incorporating active corrosion inhibitors based on lithium or praseodymium remain highly advantageous for providing long-term protection against coating damage.

Overall, these findings underscore the need for further research to: (i) improve the correlation between artificial aging tests and real-world performance, (ii) address corrosion challenges arising from galvanic coupling and (iii) develop coating systems that provide reliable, long-term corrosion protection across a broad range of environmental conditions and assembly configurations.

CRediT authorship contribution statement

A.J. Cornet: Writing – original draft, Visualization, Methodology, Investigation, Formal analysis, Data curation, Conceptualization. **A.M. Homborg:** Writing – review & editing, Supervision. **L.'t Hoen-Velterop:** Writing – review & editing, Supervision, Data curation. **J.M.C Mol:** Writing – review & editing, Supervision.

Declaration of competing interest

The authors declare that they have no known competing financial interests or personal relationships that could have appeared to influence the work reported in this paper.

Acknowledgment

The Logistic Centre Woensdrecht of the Royal Netherlands Air Force is gratefully acknowledged for enabling this research and accommodating the research work, respectively.

Data availability

Data will be made available on request.

References

[1] P.F. Taylor, L.C. Hanson, T.J. Barnes, A brief history of aircraft loads analysis methods, in: Collection of Technical Papers - AIAA/ASME/ASCE/AHS/ASC Structures, Structural Dynamics and Materials Conference, 2003. https://doi.org/10.2514/6.2003-1892.
[2] W. Corbett, Qualification Testing for Coating System Selection, in: Protective Organic Coatings, 2018. https://doi.org/10.31399/asm.hb.v05b.a0006026.
[3] MIL-PRF-23377K, PERFORMANCE SPECIFICATION, PRIMER COATINGS: EPOXY, HIGH-SOLIDS, 2012. https://assist.dla.mil.
[4] R.A. Cole, Corrosion prevention in the aerospace industries, Anti-Corros. Methods Mater. 7 (1960), https://doi.org/10.1108/eb019774.
[5] A.L. Holmes, S.S. Wise, J.P. Wise, Carcinogenicity of hexavalent chromium, Indian J. Med. Res. 128 (2008).
[6] N.A. Azeez, S.S. Dash, S.N. Gummadi, V.S. Deepa, Nano-remediation of toxic heavy metal contamination: hexavalent chromium [Cr(VI)], Chemosphere 266 (2021) 129204, https://doi.org/10.1016/j.chemosphere.2020.129204.
[7] G. Bierwagen, R. Brown, D. Battocchi, S. Hayes, Active metal-based corrosion protective coating systems for aircraft requiring no-chromate pretreatment, Prog. Org. Coat. 68 (2010) 48–61, https://doi.org/10.1016/j.porgcoat.2009.10.031.
[8] O. Gharbi, S. Thomas, C. Smith, N. Birbilis, Chromate replacement: what does the future hold? npj Mater. Degrad. 2 (2018) 23–25, https://doi.org/10.1038/s41529-018-0034-5.
[9] S. Zhao, N. Birbilis, Searching for chromate replacements using natural language processing and machine learning algorithms, npj Mater. Degrad. 7 (2023), https://doi.org/10.1038/s41529-022-00319-0.
[10] R.L. Twite, G.P. Bierwagen, Review of alternatives to chromate for corrosion protection of aluminum aerospace alloys, Prog. Org. Coat. 33 (1998) 91–100, https://doi.org/10.1016/S0300-9440(98)00015-0.
[11] P. Visser, Y. Liu, H. Terryn, J.M.C. Mol, Lithium salts as leachable corrosion inhibitors and potential replacement for hexavalent chromium in organic coatings for the protection of aluminum alloys, J. Coat. Technol. Res. 13 (2016) 557–566, https://doi.org/10.1007/s11998-016-9784-6.
[12] P. Klomjit, R.G. Buchheit, Cooperative and synergistic corrosion inhibition of AA 7075-T6 by praseodymium and $CaSO_4$, Corros. Rev. 38 (2020), https://doi.org/10.1515/corrrev-2020-0032.
[13] R.J. Santucci, B. Kannan, W. Abbott, J.R. Scully, Scientific investigation of the corrosion performance of magnesium and magnesium oxide primers on Al alloy 2024-T351 in field exposures, Corrosion 75 (2019), https://doi.org/10.5006/2879.
[14] O. Knudsen, A.W.B. Skilbred, A. Løken, B. Daneshian, D. Höche, Correlations between standard accelerated tests for protective organic coatings and field performance, Mater. Today Commun. 31 (2022), https://doi.org/10.1016/j.mtcomm.2022.103729.
[15] J. Qin, J. Jiang, Y. Tao, S. Zhao, W. Zeng, Y. Shi, T. Lu, L. Guo, S. Wang, X. Zhang, G. Jie, J. Wang, M. Xiao, Sunlight tracking and concentrating accelerated weathering test applied in weatherability evaluation and service life prediction of polymeric materials: a review, Polym. Test. 93 (2021), https://doi.org/10.1016/j.polymertesting.2020.106940.

[16] F. Peltier, D. Thierry, Development of a reliable accelerated corrosion test for painted aluminum alloys used in the aerospace industry, Corrosion Mater. Degrad. 5 (2024) 427–438, https://doi.org/10.3390/cmd5030019.
[17] M.J. Schmid, Correlation between the anticorrosive performance of protective coatings under neutral salt spray testing and outdoor atmospheric and immersion exposure, Corrosion Mater. Degrad. 5 (2024) 490–512, https://doi.org/10.3390/cmd5040023.
[18] G.W. Grossman, Correlation of laboratory to natural weathering, J. Coat. Technol. 49 (1977). https://www.q-lab.com/sites/default/files/Technical_Articles/Correlation-of-Laboratory-to-Natural-Weathering.pdf.
[19] T. Zhang, T. Zhang, Y. He, Y. Wang, Y. Bi, Corrosion and aging of organic aviation coatings: a review, Chin. J. Aeronaut. 36 (2023), https://doi.org/10.1016/j.cja.2022.12.003.
[20] N. Lebozec, D. Thierry, Influence of climatic factors in cyclic accelerated corrosion test towards the development of a reliable and repeatable accelerated corrosion test for the automotive industry, Mater. Corros. 61 (2010) 845–851, https://doi.org/10.1002/maco.200905497.
[21] N. Lebozec, N. Blandin, D. Thierry, Accelerated corrosion tests in the automotive industry: a comparison of the performance towards cosmetic corrosion, Mater. Corros. 59 (2008), https://doi.org/10.1002/maco.200804168.
[22] A.E. Hughes, J.M.C. Mol, M.L. Zheludkevich, R.G. Buchheit, Active Protective Coatings (2016), https://doi.org/10.1007/978-94-017-7540-3_4.
[23] P. Hao, Y. Dun, J. Gong, S. Li, X. Zhao, Y. Tang, Y. Zuo, Research progress on protective performance evaluation and lifetime prediction of organic coatings, Anti-Corros. Methods Mater. (2024), https://doi.org/10.1108/ACMM-04-2024-2999.
[24] H. Zhu, J. Li, Advancements in corrosion protection for aerospace aluminum alloys through surface treatment, Int. J. Electrochem. Sci. 19 (2024), https://doi.org/10.1016/j.ijoes.2024.100487.
[25] A.J. Cornet, A.M. Homborg, L. 't Hoen-Velterop, J.M.C. Mol, Post-service analysis of the degradation and protective mechanisms of chromate-based structural aircraft coatings, Prog. Org. Coat. 192 (2024) 108534, https://doi.org/10.1016/J.PORGCOAT.2024.108534.
[26] A.J. Cornet, A.M. Homborg, P.R. Anusuyadevi, L. 't Hoen-Velterop, J.M.C. Mol, Unravelling corrosion degradation of aged aircraft components protected by chromate-based coatings, Eng. Fail. Anal. 159 (2024) 108070, https://doi.org/10.1016/j.engfailanal.2024.108070.
[27] F. Ahmad, M. Al AWADH, S. Noor, Optimum alternate material selection methodology for an aircraft skin, Chin. J. Aeronaut. 36 (7) (2023) 476–488, https://doi.org/10.1016/j.cja.2023.05.019.
[28] J. Dante, Accelerated Dynamic Corrosion Test method Development, Defense Technical Information Center, Alexandria, 2017. https://apps.dtic.mil/sti/citations/AD1053665.
[29] J.G. Speight, C. Corrosion, J. Naranjo, J.G. Speight, Chapter e1 - corrosion, oil and gas corrosion, Prevention (2014) e1–e24, https://doi.org/10.1016/B978-0-12-800346-6.00001-6.
[30] B. Daneshian, D. Höche, O.Ø. Knudsen, A.W.B. Skilbred, Effect of climatic parameters on marine atmospheric corrosion: correlation analysis of on-site sensors data, npj Mater. Degrad. 7 (2023), https://doi.org/10.1038/s41529-023-00329-6.
[31] J. Demo, F. Friedersdorf, Evaluation of environmental exposure and corrosive conditions within rotorcraft airframes, in: NACE - International Corrosion Conference Series, 2014.
[32] L.F.E. Jacques, Accelerated and outdoor/natural exposure testing of coatings, Prog. Poly. Sci. (oxford) 25 (2000), https://doi.org/10.1016/S0079-6700(00)00030-7.
[33] X. Chen, W. Tian, S. Li, M. Yu, J. Liu, Effect of temperature on corrosion behavior of 3003 aluminum alloy in ethylene glycol–water solution, Chin. J. Aeronaut. 29 (2016), https://doi.org/10.1016/j.cja.2015.12.017.
[34] W.D. Ganther, D.A. Paterson, C. Lewis, P. Isaacs, S. Galea, C. Meunier, G. Mangeon, I.S. Cole, Monitoring Aircraft Microclimate and Corrosion, Procedia Eng. (2017), https://doi.org/10.1016/j.proeng.2017.04.497.
[35] I. Dehri, M. Erbil, The effect of relative humidity on the atmospheric corrosion of defective organic coating materials: an EIS study with a new approach, Corros. Sci. 42 (2000), https://doi.org/10.1016/S0010-938X(99)00126-2.
[36] B. Free, G.C. Montiel, G.A. Marino, E. Schindelholz, S. Galyon Dorman, J.S.W. Locke, The effect of variable humidity on corrosion fatigue of AA7085-T7451 with surface salt deposits, npj Mater. Degrad. 8 (1) (2024) 112, https://doi.org/10.1038/s41529-024-00530-1.
[37] N. Van Den Steen, H. Simillion, O. Dolgikh, H. Terryn, J. Deconinck, An integrated modeling approach for atmospheric corrosion in presence of a varying electrolyte film, Electrochim. Acta 187 (2016), https://doi.org/10.1016/j.electacta.2015.11.010.
[38] C. Thee, L. Hao, J. Dong, X. Mu, X. Wei, X. Li, W. Ke, Atmospheric corrosion monitoring of a weathering steel under an electrolyte film in cyclic wet-dry condition, Corros. Sci. 78 (2014), https://doi.org/10.1016/j.corsci.2013.09.008.
[39] A.Y. Musa, A.B. Mohamad, A.A.H. Kadhum, E.P. Chee, Galvanic corrosion of aluminum alloy (Al2024) and copper in 1.0 M nitric acid, Int J Electrochem. Sci. 6 (2011), https://doi.org/10.1016/s1452-3981(23)18388-x.
[40] J.F. Young, Humidity control in the laboratory using salt solutions—a review, J. Appl. Chem. 17 (1967), https://doi.org/10.1002/jctb.5010170901.
[41] I. Rörig-Dalgaard, Direct measurements of the deliquescence relative humidity in salt mixtures including the contribution from metastable phases, ACS Omega (2021), https://doi.org/10.1021/acsomega.1c00538.
[42] G.S. Frankel, C.R. Clayton, R.D. Granata, M. Kendig, H.S. Isaacs, R.L. McCreery, M. Stratmann, Mechanism of Al Alloy Corrosion and the Role of Chromate Inhibitors, 2001. https://apps.dtic.mil/sti/tr/pdf/ADA399114.pdf.
[43] G.S. Frankel, R.L. McCreery, Inhibition of Al Alloy Corrosion by Chromates, Electrochem. Soc. Interface 10 (2001) 34–38, https://doi.org/10.1149/2.f06014if.
[44] B.M. Weckhuysen, I.E. Wachs, R.A. Schoonheydt, Surface chemistry and spectroscopy of chromium in inorganic oxides, Chem. Rev. 96 (1996), https://doi.org/10.1021/cr940044o.
[45] O. Lopez-Garrity, G.S. Frankel, Corrosion inhibition of aluminum Alloy 2024-T3 by praseodymium chloride, Corrosion 70 (2014) 928–941, https://doi.org/10.5006/1244.
[46] P. Klomjit, R.G. Buchheit, Localized corrosion inhibition of AA7075-T6 by calcium sulfate, Corrosion 72 (2016), https://doi.org/10.5006/1892.
[47] P. Klomjit, R.G. Buchheit, Characterization of inhibitor storage and release from commercial primers, Prog. Org. Coat. 114 (2018) 68–77, https://doi.org/10.1016/J.PORGCOAT.2017.10.005.
[48] B.L. Treu, W. Fahrenholtz, M. O'Keefe, E. Morris, R. Albers, Effect of phase on the electrochemical and morphological properties of praseodymium-based coatings, ECS Trans. 33 (2011), https://doi.org/10.1149/1.3577753.
[49] B.L. Treu, W. Pinc, W.G. Fahrenholtz, M.J. O'Keefe, E. Morris, R. Albers, Characterization of transport processes in a praseodymium-containing coating, ECS Trans. 28 (2010), https://doi.org/10.1149/1.3496434.
[50] Z. Li, P. Visser, A.E. Hughes, A. Homborg, Y. Gonzalez-Garcia, A. Mol, Review of the state of art of Li-based inhibitors and coating technology for the corrosion protection of aluminium alloys, Surf. Coat. Technol. 478 (2024) 130441, https://doi.org/10.1016/J.SURFCOAT.2024.130441.
[51] D.B. Blücher, J.E. Svensson, L.G. Johansson, The influence of CO_2, $AlCl_3 \cdot 6H_2O$, $MgCl_2 \cdot 6H_2O$, Na_2SO_4 and NaCl on the atmospheric corrosion of aluminum, Corros. Sci. 48 (2006), https://doi.org/10.1016/j.corsci.2005.05.027.
[52] S. Oesch, M. Faller, Environmental effects on materials: The effect of the air pollutants SO_2, NO_2, NO and O_3 on the corrosion of copper, zinc and aluminium. a short literature survey and results of laboratory exposures, Corros. Sci. 39 (1997), https://doi.org/10.1016/S0010-938X(97)00047-4.
[53] D. Kotnarowska, Influence of ultraviolet radiation and aggressive media on epoxy coating degradation, Prog. Org. Coat. 37 (1999), https://doi.org/10.1016/S0300-9440(99)00070-3.
[54] P.M. Natishan, W.E. O'Grady, Chloride ion interactions with oxide-covered aluminum leading to pitting corrosion: a review, J. Electrochem. Soc. 161 (2014), https://doi.org/10.1149/2.1011409jes.
[55] E. McCafferty, Sequence of steps in the pitting of aluminum by chloride ions, Corros. Sci. 45 (2003), https://doi.org/10.1016/S0010-938X(02)00231-7.
[56] B.B. Wang, Z.Y. Wang, W. Han, W. Ke, Atmospheric corrosion of aluminium alloy 2024-T3 exposed to salt lake environment in Western China, Corros. Sci. 59 (2012), https://doi.org/10.1016/j.corsci.2012.02.015.
[57] T. Zhang, Y. He, R. Cui, T. An, Long-term atmospheric corrosion of aluminum alloy 2024-T4 in a coastal environment, J. Mater. Eng. Perform. 24 (2015), https://doi.org/10.1007/s11665-015-1541-y.

[58] S. Zhang, T. Zhang, Y. He, D. Liu, J. Wang, X. Du, B. Ma, Long-term atmospheric corrosion of aluminum alloy 2024-T4 in coastal environment: Surface and sectional corrosion behavior, J. Alloy. Compd. 789 (2019) 460–471, https://doi.org/10.1016/j.jallcom.2019.03.028.
[59] G. Cainelli, G. Cardillo, Chromium Oxidations in Organic Chemistry, in: Reactivity and Structure Concepts in Organic Chemistry, 1st ed., 1984: pp. X–264. https://doi.org/https://doi.org/10.1007/978-3-642-69362-5.
[60] D. Katre Sangita, Recent advances in the oxidation reactions of organic compounds using chromium (VI) reagents, Res. J. Chem. Environ. 24 (2020).
[61] U.-E. Charles-Granville, C.F. Glover, J.R. Scully, R.G. Kelly, Effect of pH and Al cations on chromate inhibition of galvanic-induced corrosion of AA7050-T7451 macro-coupled to 316SS, J. Electrochem. Soc. 168 (2021), https://doi.org/10.1149/1945-7111/ac412a.
[62] V.N. Rafla, J.R. Scully, Effect of soluble chromate inhibitor on the macro- and meso-scale damage morphology and electrochemical corrosion behavior of AA7050-T7451 coupled to type 316 stainless steel, Corrosion 75 (2019) 587–603, https://doi.org/10.5006/2858.
[63] N.S. Sangaj, V.C. Malshe, Permeability of polymers in protective organic coatings, Prog. Org. Coat. 50 (2004), https://doi.org/10.1016/j.porgcoat.2003.09.015.
[64] T. Wang, S. Luo, C. Wang, J. Wang, C.E. Weinell, K. Dam-Johansen, J.J. Segura, E. Graversen, S. Kiil, Methanol degradation mechanisms and permeability phenomena in novolac epoxy and polyurethane coatings, J. Coat. Technol. Res. 18 (2021), https://doi.org/10.1007/s11998-020-00446-w.
[65] J. Xu, N. Geier, J. Shen, V. Krishnaraj, S. Samsudeensadham, A review on CFRP drilling: fundamental mechanisms, damage issues, and approaches toward high-quality drilling, J. Mater. Res. Technol. 24 (2023), https://doi.org/10.1016/j.jmrt.2023.05.023.
[66] J.J.H.M. Es, L. 't Hoen-Velterop, Towards understanding of corrosion on composite aircraft, NATO STO J. (2019) 1–13.
[67] X.F. Yang, C. Vang, D.E. Tallman, G.P. Bierwagen, S.G. Croll, S. Rohlik, Weathering degradation of a polyurethane coating, Polym. Degrad. Stab. 74 (2001), https://doi.org/10.1016/S0141-3910(01)00166-5.
[68] T. Gao, Z. He, L.H. Hihara, H.S. Mehr, M.D. Soucek, Outdoor exposure and accelerated weathering of polyurethane/polysiloxane hybrid coatings, Prog. Org. Coat. 130 (2019), https://doi.org/10.1016/j.porgcoat.2019.01.046.
[69] F. Awaja, P.J. Pigram, Surface molecular characterisation of different epoxy resin composites subjected to UV accelerated degradation using XPS and ToF-SIMS, Polym. Degrad. Stab. 94 (2009), https://doi.org/10.1016/j.polymdegradstab.2009.01.001.
[70] E. Schindelholz, R.G. Kelly, Wetting phenomena and time of wetness in atmospheric corrosion: a review, Corros. Rev. 30 (2012), https://doi.org/10.1515/corrrev-2012-0015.
[71] R. Black, R. Cusic, MIL-STD-889 and the Impacts on Corrosion Prevention, NATO STO J. (2023) 0901–0912, in: https://www.sto.nato.int/publications/STO%20Meeting%20Proceedings/STO-MP-AVT-373/MP-AVT-373-09.pdf.
[72] O. Schneider, R.G. Kelly, Localized coating failure of epoxy-coated aluminium alloy 2024-T3 in 0.5 M NaCl solutions: correlation between coating degradation, blister formation and local chemistry within blisters, Corros. Sci. 49 (2007) 594–619, https://doi.org/10.1016/j.corsci.2006.06.006.
[73] S. Effendy, T. Zhou, H. Eichman, M. Petr, M.Z. Bazant, Blistering failure of elastic coatings with applications to corrosion resistance, Soft Matter 17 (2021) 9480–9498, https://doi.org/10.1039/d1sm00986a.
[74] W. Funke, Blistering of paint films and filiform corrosion, Prog. Org. Coat. 9 (1981), https://doi.org/10.1016/0033-0655(81)80014-3.
[75] C.A. Matzdorf, W.C. Nickerson, B.C. Rincon Troconis, G.S. Frankel, L. Li, R.G. Buchheit, Galvanic test panels for accelerated corrosion testing of coated Al alloys: Part 1 - Concept, Corrosion 69 (2013), https://doi.org/10.5006/0905.
[76] D.E. Floyd, D.E. Peerman, H. Wittcoff, Characteristics of the polyamide-epoxy resin system, J. Appl. Chem. 7 (1957), https://doi.org/10.1002/jctb.5010070507.
[77] K.B. Tator, Epoxy Resins and Curatives, in: Protective Organic Coatings, 2018. https://doi.org/10.31399/asm.hb.v05b.a0006077.
[78] C.W. Extrand, Water contact angles and hysteresis of polyamide surfaces, J. Colloid Interf. Sci. 248 (2002), https://doi.org/10.1006/jcis.2001.8172.
[79] T.P. Hoar, The production and breakdown of the passivity of metals, Corros. Sci. 7 (1967), https://doi.org/10.1016/S0010-938X(67)80023-4.
[80] Z. Rajabimashhadi, R. Naghizadeh, A. Zolriasatein, S. Bagheri, C. Mele, C. Esposito Corcione, Hydrophobic, mechanical, and physical properties of polyurethane nanocomposite: synergistic impact of $Mg(OH)_2$ and SiO_2, Polymers 15 (8) (2023) 1916, https://doi.org/10.3390/polym15081916.
[81] S. Rabbani, E. Bakhshandeh, R. Jafari, G. Momen, Superhydrophobic and icephobic polyurethane coatings: fundamentals, progress, challenges and opportunities, Prog. Org. Coat. 165 (2022), https://doi.org/10.1016/j.porgcoat.2022.106715.
[82] M. Amrollahi, G.M.M. Sadeghi, Assessment of adhesion and surface properties of polyurethane coatings based on non-polar and hydrophobic soft segment, Prog. Org. Coat. 93 (2016), https://doi.org/10.1016/j.porgcoat.2015.12.001.
[83] H.R. Jeon, J.H. Park, M.Y. Shon, Corrosion protection by epoxy coating containing multi-walled carbon nanotubes, J. Ind. Eng. Chem. 19 (2013), https://doi.org/10.1016/j.jiec.2012.10.030.